**S E P A R A T A**

*Revista Geológica de Chile 35 (1): 123-145. January, 2008*

***Revista Geológica de Chile***

# Geochronology of the Lower Cretaceous volcanism from the Coastal Range (29°20'-30°S), Chile

**Diego Morata[1], Gilbert Féraud[2], Luis Aguirre[1], Gloria Arancibia[3], Mauricio Belmar[1], Salvador Morales[4], Javier Carrillo[5]**

[1] *Departamento de Geología, Facultad de Ciencias Físicas y Matemáticas, Universidad de Chile, Plaza Ercilla 803, Santiago, Chile. dmorata@cec.uchile.cl; luaguirr@cec.uchile.cl; mbelmar@ing.uchile.cl*

[2] *Geosciences Azur, UMR 6526. CNRS-Université de Nice-Sophia Antipolis, 06108 Nice cedex 02, France. Gilbert.FERAUD@unice.fr*

[3] *La Quilla 659, Ñuñoa, Santiago, Chile. gloarancibia@123.cl*

[4] *Departamento de Mineralogía-Petrología e Instituto Andaluz de Ciencias de la Tierra, CSIC-Universidad de Granada, Facultad de Ciencias, Avda. Fuentenueva s/n, 18002 Granada, España. smorales@ugr.es*

[5] *Departamento de Didáctica de las Ciencias Experimentales, Facultad de Ciencias de la Educación, Campus Universitario de Cartuja, 18071 Granada, España. fjcarril@ugr.es*

ISSN 0716-0208
Editada por el Servicio Nacional de Geología y Minería
con la colaboración científica de la Sociedad Geológica de Chile
Avda. Santa María 0104, Casilla 10465, Santiago, Chile.
revgeologica@sernageomin.cl; http://www.scielo.cl/rgch.htm; http://www.sernageomin.cl

*Revista Geológica de Chile 35 (1): 123-145. January, 2008*

***Revista Geológica de Chile***

*www.scielo.cl/rgch.htm*

# Geochronology of the Lower Cretaceous volcanism from the Coastal Range (29°20'-30°S), Chile

**Diego Morata[1], Gilbert Féraud[2], Luis Aguirre[1], Gloria Arancibia[3], Mauricio Belmar[1], Salvador Morales[4], Javier Carrillo[5]**

[1] *Departamento de Geología, Facultad de Ciencias Físicas y Matemáticas, Universidad de Chile, Plaza Ercilla 803, Santiago, Chile. dmorata@cec.uchile.cl; luaguirr@cec.uchile.cl; mbelmar@ing.uchile.cl*

[2] *Geosciences Azur, UMR 6526. CNRS-Université de Nice-Sophia Antipolis, 06108 Nice cedex 02, France. Gilbert.FERAUD@unice.fr*

[3] *La Quilla 659, Ñuñoa, Santiago, Chile. gloarancibia@123.cl*

[4] *Departamento de Mineralogía-Petrología e Instituto Andaluz de Ciencias de la Tierra, CSIC-Universidad de Granada, Facultad de Ciencias, Avda. Fuentenueva s/n, 18002 Granada, España. smorales@ugr.es*

[5] *Departamento de Didáctica de las Ciencias Experimentales, Facultad de Ciencias de la Educación, Campus Universitario de Cartuja, 18071 Granada, España. fjcarril@ugr.es*

**ABSTRACT.** $^{40}Ar/^{39}Ar$ age data (laser and furnace step heating) on plagioclase from Lower Cretaceous volcanic sequences from the Arqueros Formation in two sections of the Coastal Range at the latitude of La Serena (≈29°S) have been obtained. Due to the partial alteration of plagioclase crystals, disturbed age spectra in the furnace experiments have been observed, whereas laser heating determinations involving a much smaller quantity of grains carefully selected, could display plateau ages corresponding to pure plagioclase, as demonstrated by a constant $^{37}Ar_{Ca}/^{39}Ar_{K}$ ratio. Plateau ages of 114.1±0.5 Ma (sample ARQ99-4), 111.3±0.9 Ma (sample TC99-5a), and 91.0±0.6 Ma (sample TC99-2) were found in lava flows, and 84.3±1.3 Ma on a dyke (sample ARQ99-7). These new $^{40}Ar/^{39}Ar$ ages, together with those previously published in central Chile, allow a constriction of the extensional magmatism during the Early Cretaceous in the Coastal Range of central and north-central Chile. All these data are in accordance with a long lived Early Cretaceous Magmatic Province (119-84 Ma), that could have started with a brief and huge magmatic event, mostly developed in the central part of the Coastal Range, followed by discrete magmatic pulses at further northern latitudes.

*Keywords: $^{40}Ar/^{39}Ar$ dating, Plagioclase, Lower Cretaceous, Volcanism, Coastal Range, Chile.*

**RESUMEN. Geocronología del volcanismo del Cretácico Inferior en la Cordillera de la Costa (29°20'-30°S), Chile.** Se han obtenido edades $^{40}Ar/^{39}Ar$ (calentamiento por pasos en horno y mediante láser) en plagioclasas de secuencias volcánicas de dos secciones del Cretácico Inferior de la Cordillera de la Costa (Formación Arqueros) a la latitud de La Serena (≈29°S). Debido a la alteración parcial de los cristales de plagioclasa, se han observado espectros de edades perturbados en las medidas realizadas en horno. Sin embargo, en las determinaciones realizadas mediante láser en unos pocos granos de plagioclasa meticulosamente seleccionados se han obtenido edades plateau correspondientes a plagioclasa primaria, como lo evidencian los valores constantes de la relación $^{37}Ar_{Ca}/^{39}Ar_{K}$. Se han obtenido edades plateau de 114,1±0,5 Ma (muestra ARQ99-4), 111,3±0,9 Ma (muestra TC99-5a) y 91,0±0,6 Ma (muestra TC99-2) en diferentes coladas de lava, y de 84,3±1,3 Ma en un dique (muestra ARQ99-7). Estas nuevas edades $^{40}Ar/^{39}Ar$, junto a las ya publicadas en Chile central, permiten constreñir mejor la duración del evento magmático extensional durante el Cretácico Inferior en la Cordillera de la Costa del centro y centro-norte de Chile. Estos datos están de acuerdo con la existencia de una Provincia Magmática del Cretácico Inferior (119-84 Ma), que habría comenzado con un breve e intenso evento magmático en la zona central de la Cordillera seguido de pulsos magmáticos discretos hacia latitudes más septentrionales.

*Palabras claves: Geocronología $^{40}Ar/^{39}Ar$, Plagioclasa, Cretácico Inferior, Volcanismo, Cordillera de la Costa, Chile.*

## 1. Introduction

The Mesozoic-Cenozoic geological evolution of north-central Chile is characterized by the eastward migration of the magmatic arc which resulted in the production of plutonic and volcanic rocks which mostly conform both the Coastal Range (to the west) and the High Andes (to the east). Precise dating of the different magmatic events is a key point to understand the evolution of this active margin. During the Early Cretaceous, volcanism in the Coastal Range of central and north-central Chile was characterized by the emplacement of thick piles of highly porphyritic plagioclase-rich calc-alkaline to high-K calc-alkaline andesites and basaltic andesites, locally known as 'ocoites' (*e.g.*, Aguirre, 1985) best represented by the Veta Negra Formation. The mineralogy and geochemistry of these lavas are highly homogeneous, conforming a magmatic province of several hundred cubic kilometers (Levi *et al*., 1988; Vergara *et al*., 1995; Morata *et al*., 2001; Morata and Aguirre, 2003). Moreover, a pervasive and non-deformative very low to low-grade metamorphism affects these rocks, preserving the primary structures and textures but partially modifying the primary mineral chemistry (Aguirre *et al*., 1989; Levi *et al*., 1989; Aguirre *et al*., 1999). Precise dating of these basic volcanic rocks, dominated by pyroxene, plagioclase±olivine as phenocrysts, is limited by a strong alteration affecting most of the rocks and its phenocrysts. Dating of carefully selected plagioclase crystals by the step heating $^{40}Ar/^{39}Ar$ method seems to be the best way to obtain valid and accurate ages, although their frequent alteration to sericite hinders the obtention of primary (crystallization) plateau ages. This approach was successfully applied by Aguirre *et al*. (1999) and Fuentes *et al*. (2001, 2005) to a few carefully selected plagioclase grains from those basic volcanic rocks from central Chile.

In spite of the large geographical extent of the Lower Cretaceous volcanism, only few geochronological data are available. Previous K-Ar ages (errors at the 2σ level) were restricted to the Lower Cretaceous volcanic rocks from the Veta Negra Formation, few kilometres north of Santiago (105±2 Ma (plagioclase), Drake *et al*., 1982; 110±4 Ma to 113±4 Ma ('fresh' whole-rock) Munizaga *et al*., 1988; 94±2 Ma (plagioclase) and 100±3 Ma to 115±4 Ma (whole-rock), Rivano *et al*., 1996). Boric and Munizaga (1994) obtained a $^{40}Ar/^{39}Ar$ plateau age of 131.8±3.1 Ma on plagioclase from a trachytic dyke from the El Soldado mine, hosted in the acid upper level of the Lo Prado Formation, the oldest Lower Cretaceous unit in the Coastal Range of central Chile. More recent $^{40}Ar/^{39}Ar$ plateau ages of 119.4±1.2 Ma (Aguirre *et al*., 1999) and 118.7±0.6 Ma (Fuentes *et al*., 2001, 2005) were obtained on fresh plagioclases from lavas belonging to the overlying Veta Negra Formation (Lower Cretaceous) in the Bustamante (33°25') and Chacana (33°S) areas, respectively.

Here we report nine $^{40}Ar/^{39}Ar$ age data on plagioclase from Lower Cretaceous volcanic sequences in two sections of the Coastal Range at the latitude of La Serena (≈29°S), which correlate with lavas of the Veta Negra Formation in central Chile. Rb/Sr and Sm/Nd isochron dating was also carried out in one of these volcanic rocks. These new ages, together with those previously obtained in rocks from the Coastal Range west from Santiago, would allow to define a Lower Cretaceous Magmatic Province (LCMP) and relate it to the evolution of the Chilean Pacific margin during the Cretaceous.

## 2. Geological setting

The Chilean Pacific margin has been a continuous subduction zone from the Jurassic up to now, with variations in the nature of the related magmatism as a consequence of major tectonic constraints. During the Early Cretaceous in central Chile, a volcanic arc was formed within the continental margin on eroded Jurassic and pre-Jurassic rocks, conforming a *ca.* 1,000 km northern-southern belt, 100 to 150 km wide and up to 13 km thick in some of its sections (*e.g.*, Vergara *et al*., 1995). Thick, predominantly volcanic sequences crop out along the western border of the belt (the Coastal Range), whereas sedimentary rocks with subordinate volcanic rocks appear to the east (the Andean Range) (Aguirre, 1985). An intra-arc extensional basin, subsiding at high rates (100-300 m/m.y.), has been proposed as the geodynamic setting for the Coastal Range during the Early Cretaceous (Vergara *et al*., 1995) whereas for the Andean Range Vergara and Nyström (1996) have postulated a back-arc setting for the same period.

The Lower Cretaceous record in the Coastal Range at 29-30°S latitude is characterized by stratified sequences of volcanic (mostly porphyritic andesites and basaltic andesites) and sedimentary rocks (Fig. 1). Volcanic rocks dominate in the Arqueros Formation (Hauterivian-Barremian; Aguirre

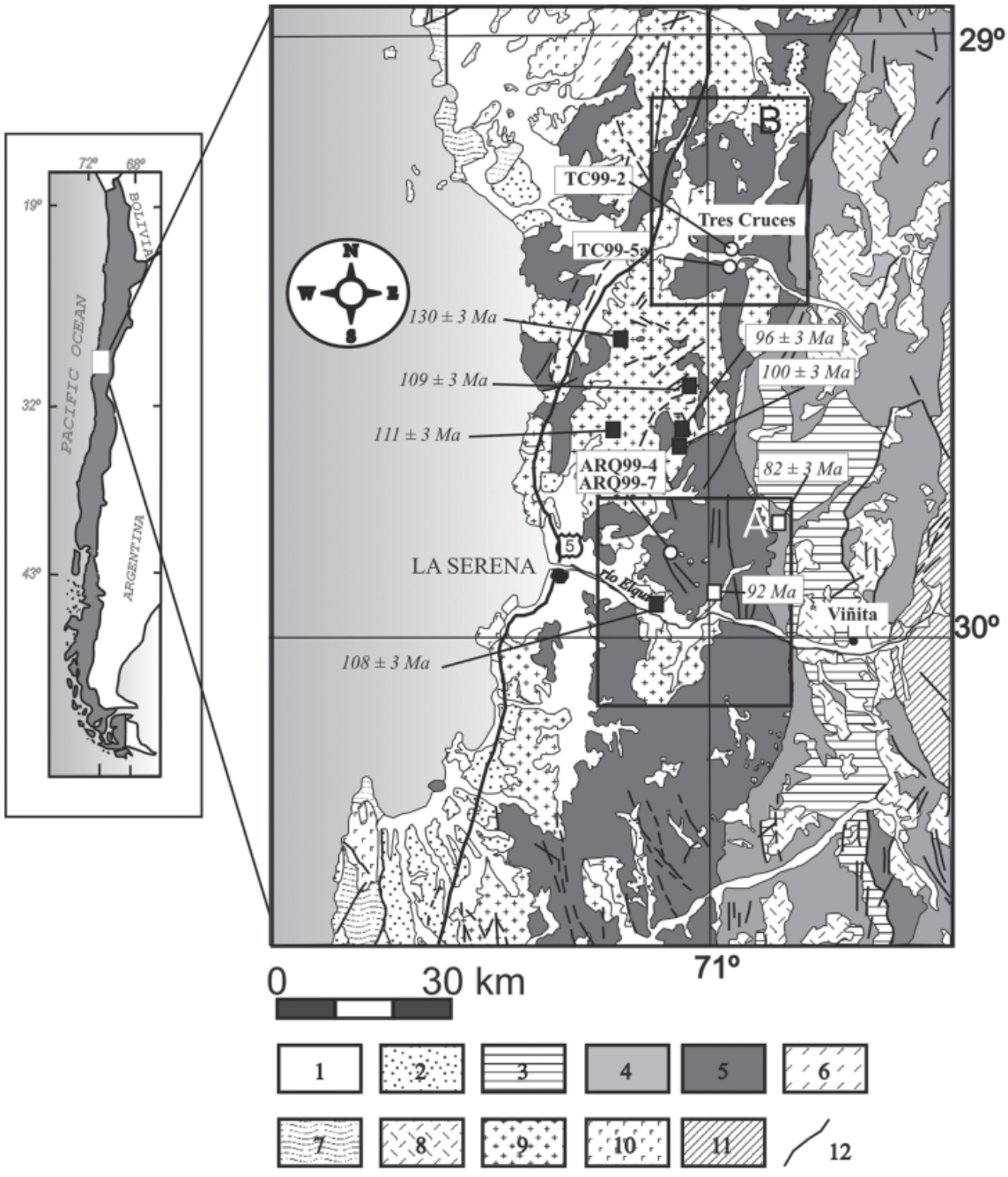


FIG. 1. Geological map (modified and simplified from the SERNAGEOMIN, 1982) showing the two studied areas (A and B) of the Lower Cretaceous volcanic rocks from the Coastal Range in La Serena region (30ºS) and location of dated samples. UTM coordinates (South American 1956 datum): sample ARQ99-4: 0312412, 6701483; ARQ99-7: 0311527, 6701907; TC99-2: 0312100, 6749834; TC99-5309874, 6749163. Previous ages of plutonic rocks (error at the 2σ level, Emparan and Pineda, 2000) and Upper Cretaceous volcanic rocks (Pineda and Emparan, 1997) are shown. Legend: **1.** Quaternary sediments; **2.** Mio-Pliocene marine sediments; **3.** Paleocene-Eocene continental volcanic and sedimentary rocks; **4.** Lower Tertiary-Upper Cretaceous volcanic and sedimentary rocks; **5.** Lower Cretaceous volcanic and sedimentary rocks; **6.** Middle-Upper Triassic volcanic and sedimentary rocks; **7.** Paleozoic metamorphic rocks; **8.** Tertiary plutonic rocks; **9.** Lower Tertiary-Upper Cretaceous plutonic rocks; **10.** Jurassic plutonic rocks; **11.** Andean Cordillera; **12.** Faults. **White square:** K-Ar on whole rock; **black square:** K-Ar on biotite.

and Egert, 1965), whereas the overlying Quebrada Marquesa Formation (Upper Barremian-Albian; Aguirre and Egert, 1965), is mainly composed of tuffs and breccias with minor marine intercalations, and continental volcaniclastic rocks and andesitic lavas, mostly present at their basal units. The presence of pillow-lava structures in some of the oldest lava flows of the Arqueros Formation (Aguirre and Egert, 1965) indicates a partially subaquatic emplacement. Above the Quebrada Marquesa Formation, mainly continental clastic rocks, lavas and breccias of the Upper Cretaceous Viñita Formation (Aguirre and Egert, 1965, 1970) are unconformably deposited. According to paleogeographic reconstructions, marine basin deposition in the north-central Chile would has been developed during the Barremian-Aptian (Mourgues, 2004), in agreement with the presence of evaporitic lithologies in the upper levels of the Arqueros Formation (Aguirre and Egert, 1965).

Previous radiometric ages in this area are scarce and mostly centered on intrusives. Based on palaeontological evidences, a Late Hauterivian-Late Barremian age (≈120-125 Ma) has been proposed for the Arqueros Formation (Aguirre and Egert, 1965). A K-Ar whole-rock age of ≈92 Ma obtained on a lava flow of the overlaying Quebrada Marquesa Formation, along the Quebrada Marquesa valley (Fig. 1) was considered as a minimum age due to the pervasive secondary alteration of the rock (Palmer *et al*., 1980). An U-Pb zircon age of 107.0±0.6 Ma has been recently obtained by Emparan and Pineda (2006) in ignimbrites from the upper part of this formation, some kilometres south of the studied area. Finally, a K-Ar whole-rock age of 82±3 Ma obtained on a lava flow of the Upper Cretaceous Viñita Formation (Fig.1) was also interpreted as a minimum age due the pervasive alteration affecting these rocks (Pineda and Emparan, 1997; Emparan and Pineda, 1999).

The Lower Cretaceous volcano-sedimentary sequences are slightly folded, block-faulted, and locally intruded by calc-alkaline and oversaturated granitoids. 'Whole-rock' and biotite K-Ar ages (error at the 2σ level), obtained from the composite Santa Gracia Pluton, range from 130±3 Ma to 96±3 Ma (Emparan and Pineda, 2000), the youngest ages corresponding to rocks from the eastern border of the pluton. Other granodiorite plutons with biotite K-Ar ages of 109±3 and 108±3 Ma (Emparan and Pineda, 2000 and references therein) intruding the lower units of the Arqueros Formation give a minimum age for these sequences (Fig. 1).

Samples dated in this study were collected in two different sections at *ca*. 500 km north from Santiago: the Llano de Arqueros (sector A in Fig. 1) and the Tres Cruces areas (sector B). In both areas, volcanic rocks are intercalated with shallow-water marine sedimentary rocks. In sector A, the samples are from a porphyritic andesite (sample ARQ99-4) from the $Ka_3$ member of the Arqueros Formation (according to Aguirre and Egert, 1965) and from a porphyritic andesitic dyke (sample ARQ99-7) cutting lavas of the $Ka_1$ member of that formation. In sector B, the analysed rocks (TC99-2 and TC99-5a) belong to units palaeontologically and biostratigraphycally correlatable with the Arqueros Formation (Aguirre and Egert, 1965; Moscoso, 1976; Mourgues, 2000a, b).

## 3. Analytical methods

With the aim to check the mineral composition as well as the presence of impurities or inclusions in primary minerals of the dated samples, microanalyses and electron back-scattered images were performed. Mineral compositions (Tables 1 and 2) were determined using a CAMECA SX-50 microprobe (20 nA, 20 kV, 5 μm as analytical conditions and natural and synthetic-certified standards for calibration of quantitative analysis) and a Zeiss DSM 950 scanning electron microscope (SEM) equipped with an Oxford Isis 300 X-ray energy dispersive (EDX) microanalysis system (2-5 nA, 20kV, and natural silicates as standards) at the 'Centro de Instrumentación Científica, Universidad de Granada, España'. Back-scattered electron images were carried out with this Zeiss DSM 950 SEM and also using a Philips XL30 SEM, with operating software version 5.0, upgraded to version 5.39, 20 keV energy and a size spot of 5.5 μm (University of Liverpool, UK).

For the isotopic measurements, plagioclase and clinopyroxene were separated using standard crushing, heavy liquids and Frantz isodynamic methods at the 'Departamento de Geología, Universidad de Chile'. Whole-rock isotopic measurements were carried out on agate crushed samples of previously cleaned chips of rocks. For $^{40}Ar/^{39}Ar$ dating, plagioclases were then carefully selected by hand-picking under a binocular microscope in order to prevent the presence of altered grains in mineral separates. Plagioclase separates were irradiated in position 5c for 70 h in the nuclear reactor of McMaster University, Hamilton, Canada. The total neutron flux density during irradiation was $8.8x10^{18}$ n $cm^{-2}$, with

**TABLE 1. MICROPROBE ANALYSES OF PLAGIOCLASE PHENOCRYSTS.**

| Sample | ARQ994 | ARQ994 | ARQ994 | ARQ994 | ARQ994 | ARQ997 | ARQ997 | ARQ997 | ARQ997 | TC992 | TC992 | TC992 | TC992 | TC992 |
|---|---|---|---|---|---|---|---|---|---|---|---|---|---|---|
| **Analysis** | **1** | **2** | **3** | **5** | **14** | **25** | **28** | **29** | **30** | **89** | **90** | **91** | **93** | **94** |
| $SiO_2$ | 53.63 | 53.45 | 62.72 | 52.83 | 52.78 | 50.18 | 52.40 | 51.82 | 49.25 | 54.30 | 55.16 | 55.84 | 57.63 | 55.18 |
| $TiO_2$ | 0.08 | 0.05 | 0.02 | 0.05 | 0.06 | 0.05 | 0.08 | 0.08 | 0.05 | 0.04 | 0.06 | 0.04 | 0.22 | 0.05 |
| $Al_2O_3$ | 27.92 | 28.06 | 22.53 | 28.02 | 28.37 | 28.24 | 28.97 | 28.57 | 27.57 | 28.29 | 28.04 | 27.60 | 26.35 | 28.00 |
| $Cr_2O_3$ | 0.00 | 0.01 | 0.00 | 0.00 | 0.00 | 0.00 | 0.00 | 0.00 | 0.00 | 0.00 | 0.00 | 0.00 | 0.01 | 0.00 |
| FeO | 0.89 | 0.81 | 0.39 | 0.83 | 0.80 | 0.75 | 0.75 | 0.72 | 0.59 | 0.58 | 0.47 | 0.45 | 0.57 | 0.41 |
| MnO | 0.02 | 0.00 | 0.02 | 0.03 | 0.00 | 0.00 | 0.01 | 0.02 | 0.00 | 0.01 | 0.00 | 0.00 | 0.02 | 0.00 |
| MgO | 0.11 | 0.10 | 0.16 | 0.14 | 0.11 | 0.15 | 0.14 | 0.14 | 0.13 | 0.06 | 0.07 | 0.06 | 0.07 | 0.06 |
| CaO | 11.21 | 11.32 | 3.90 | 11.47 | 11.72 | 11.45 | 11.91 | 11.96 | 10.82 | 11.20 | 10.63 | 10.19 | 9.39 | 10.66 |
| $Na_2O$ | 4.55 | 4.46 | 8.80 | 4.36 | 4.37 | 4.08 | 4.22 | 3.96 | 4.03 | 4.99 | 5.22 | 5.36 | 5.48 | 5.23 |
| $K_2O$ | 0.73 | 0.72 | 0.10 | 0.70 | 0.68 | 0.34 | 0.40 | 0.41 | 0.35 | 0.44 | 0.50 | 0.59 | 0.69 | 0.54 |
| Total | 99.15 | 98.99 | 98.66 | 98.43 | 98.89 | 95.24 | 98.89 | 97.67 | 92.79 | 99.92 | 100.15 | 100.13 | 100.41 | 100.12 |
| **Structural formulae to 8 oxygens** | | | | | | | | | | | | | | |
| Si | 2.458 | 2.453 | 2.808 | 2.441 | 2.429 | 2.395 | 2.408 | 2.410 | 2.407 | 2.463 | 2.490 | 2.517 | 2.582 | 2.491 |
| Ti | 0.003 | 0.002 | 0.001 | 0.002 | 0.002 | 0.002 | 0.003 | 0.003 | 0.002 | 0.001 | 0.002 | 0.001 | 0.007 | 0.002 |
| Al | 1.508 | 1.517 | 1.189 | 1.526 | 1.538 | 1.588 | 1.569 | 1.566 | 1.587 | 1.512 | 1.492 | 1.466 | 1.391 | 1.490 |
| Cr | 0.000 | 0.000 | 0.000 | 0.000 | 0.000 | 0.000 | 0.000 | 0.000 | 0.000 | 0.000 | 0.000 | 0.000 | 0.000 | 0.000 |
| $Fe^{2+}$ | 0.034 | 0.031 | 0.015 | 0.032 | 0.031 | 0.030 | 0.029 | 0.028 | 0.024 | 0.022 | 0.018 | 0.017 | 0.021 | 0.015 |
| $Mn^{2+}$ | 0.001 | 0.000 | 0.001 | 0.001 | 0.000 | 0.000 | 0.001 | 0.001 | 0.000 | 0.000 | 0.000 | 0.000 | 0.001 | 0.000 |
| Mg | 0.008 | 0.007 | 0.011 | 0.009 | 0.007 | 0.010 | 0.009 | 0.010 | 0.009 | 0.004 | 0.005 | 0.004 | 0.005 | 0.004 |
| Ca | 0.551 | 0.557 | 0.187 | 0.568 | 0.578 | 0.585 | 0.586 | 0.596 | 0.566 | 0.544 | 0.514 | 0.492 | 0.450 | 0.516 |
| Na | 0.404 | 0.396 | 0.764 | 0.391 | 0.390 | 0.377 | 0.376 | 0.357 | 0.382 | 0.439 | 0.456 | 0.469 | 0.476 | 0.457 |
| K | 0.043 | 0.042 | 0.006 | 0.041 | 0.040 | 0.021 | 0.024 | 0.024 | 0.022 | 0.025 | 0.029 | 0.034 | 0.039 | 0.031 |
| Sum | 5.009 | 5.006 | 4.982 | 5.010 | 5.015 | 5.008 | 5.005 | 4.995 | 4.999 | 5.012 | 5.005 | 5.000 | 4.973 | 5.007 |
| $^{37}ArCa/^{39}ArK$ | 7.015 | 7.239 | 17.491 | 7.572 | 7.904 | 15.465 | 13.501 | 13.399 | 14.313 | 11.757 | 9.761 | 7.905 | 6.262 | 9.045 |
| An | 55.198 | 55.949 | 19.558 | 56.795 | 57.365 | 59.517 | 59.464 | 60.963 | 58.402 | 53.965 | 51.444 | 49.459 | 46.648 | 51.347 |
| Ab | 40.502 | 39.828 | 79.831 | 39.106 | 38.669 | 38.380 | 38.129 | 36.551 | 39.368 | 43.527 | 45.676 | 47.122 | 49.282 | 45.552 |
| Or | 4.300 | 4.223 | 0.611 | 4.099 | 3.966 | 2.103 | 2.407 | 2.486 | 2.230 | 2.508 | 2.880 | 3.419 | 4.070 | 3.102 |

Table 1 (continued).

| Sample | TC992 | TC992 | TC992 | TC992 | TC992 | TC992 | TC992 | TC992 | TC992 | TC992 | TC992 | TC992 | TC992 | TC992 | TC992 |
|---|---|---|---|---|---|---|---|---|---|---|---|---|---|---|---|
| **Analysis** | **95** | **96** | **98** | **100** | **107** | **109** | **110** | **111** | **112** | **115** | **116** | **117** | **119** | **120** | **123** |
| $SiO_2$ | 54.59 | 56.28 | 55.92 | 53.80 | 53.43 | 52.98 | 51.56 | 54.59 | 55.30 | 55.05 | 56.10 | 56.40 | 53.97 | 56.08 | 55.36 |
| $TiO_2$ | 0.05 | 0.04 | 0.06 | 0.06 | 0.07 | 0.03 | 0.04 | 0.05 | 0.07 | 0.06 | 0.05 | 0.06 | 0.05 | 0.05 | 0.05 |
| $Al_2O_3$ | 27.48 | 27.08 | 27.52 | 28.77 | 28.69 | 29.55 | 30.11 | 28.57 | 28.04 | 28.15 | 27.36 | 27.30 | 28.75 | 27.71 | 27.99 |
| $Cr_2O_3$ | 0.00 | 0.00 | 0.00 | 0.00 | 0.02 | 0.00 | 0.01 | 0.01 | 0.01 | 0.00 | 0.01 | 0.00 | 0.00 | 0.00 | 0.00 |
| FeO | 0.47 | 0.51 | 0.48 | 0.47 | 0.54 | 0.47 | 0.71 | 0.55 | 0.55 | 0.53 | 0.47 | 0.45 | 0.61 | 0.55 | 0.49 |
| MnO | 0.00 | 0.00 | 0.00 | 0.00 | 0.00 | 0.00 | 0.01 | 0.00 | 0.00 | 0.00 | 0.00 | 0.00 | 0.00 | 0.00 | 0.00 |
| MgO | 0.07 | 0.04 | 0.06 | 0.05 | 0.05 | 0.04 | 0.10 | 0.07 | 0.05 | 0.06 | 0.06 | 0.05 | 0.08 | 0.07 | 0.05 |
| CaO | 10.32 | 9.77 | 10.08 | 11.65 | 11.83 | 12.53 | 13.43 | 11.36 | 10.65 | 10.82 | 10.01 | 9.68 | 11.57 | 10.21 | 10.60 |
| $Na_2O$ | 5.35 | 5.70 | 5.45 | 4.81 | 4.80 | 4.35 | 3.78 | 4.95 | 5.27 | 5.12 | 5.48 | 5.68 | 4.87 | 5.55 | 5.26 |
| $K_2O$ | 0.51 | 0.66 | 0.64 | 0.38 | 0.40 | 0.38 | 0.29 | 0.46 | 0.54 | 0.51 | 0.63 | 0.72 | 0.41 | 0.53 | 0.56 |
| Total | 98.83 | 100.08 | 100.20 | 99.98 | 99.84 | 100.33 | 100.03 | 100.62 | 100.47 | 100.29 | 100.16 | 100.34 | 100.30 | 100.75 | 100.36 |
| **Structural formulae to 8 oxygens** | | | | | | | | | | | | | | | |
| Si | 2.497 | 2.538 | 2.519 | 2.440 | 2.431 | 2.400 | 2.351 | 2.459 | 2.490 | 2.483 | 2.527 | 2.536 | 2.442 | 2.514 | 2.494 |
| Ti | 0.002 | 0.001 | 0.002 | 0.002 | 0.003 | 0.001 | 0.001 | 0.002 | 0.002 | 0.002 | 0.002 | 0.002 | 0.002 | 0.002 | 0.002 |
| Al | 1.482 | 1.439 | 1.461 | 1.538 | 1.538 | 1.578 | 1.619 | 1.517 | 1.488 | 1.497 | 1.453 | 1.446 | 1.533 | 1.464 | 1.486 |
| Cr | 0.000 | 0.000 | 0.000 | 0.000 | 0.001 | 0.000 | 0.000 | 0.001 | 0.000 | 0.000 | 0.000 | 0.000 | 0.000 | 0.000 | 0.000 |
| $Fe^{2+}$ | 0.018 | 0.019 | 0.018 | 0.018 | 0.021 | 0.018 | 0.027 | 0.021 | 0.021 | 0.020 | 0.018 | 0.017 | 0.023 | 0.020 | 0.018 |
| $Mn^{2+}$ | 0.000 | 0.000 | 0.000 | 0.000 | 0.000 | 0.000 | 0.000 | 0.000 | 0.000 | 0.000 | 0.000 | 0.000 | 0.000 | 0.000 | 0.000 |
| Mg | 0.005 | 0.003 | 0.004 | 0.003 | 0.003 | 0.003 | 0.007 | 0.005 | 0.003 | 0.004 | 0.004 | 0.003 | 0.005 | 0.005 | 0.004 |
| Ca | 0.506 | 0.472 | 0.486 | 0.566 | 0.577 | 0.608 | 0.656 | 0.548 | 0.514 | 0.523 | 0.483 | 0.466 | 0.561 | 0.490 | 0.512 |
| Na | 0.474 | 0.499 | 0.476 | 0.423 | 0.423 | 0.382 | 0.334 | 0.433 | 0.460 | 0.447 | 0.478 | 0.496 | 0.427 | 0.482 | 0.459 |
| K | 0.030 | 0.038 | 0.037 | 0.022 | 0.023 | 0.022 | 0.017 | 0.026 | 0.031 | 0.029 | 0.036 | 0.042 | 0.023 | 0.030 | 0.032 |
| Sum | 5.013 | 5.009 | 5.004 | 5.012 | 5.020 | 5.012 | 5.013 | 5.010 | 5.009 | 5.005 | 5.002 | 5.008 | 5.015 | 5.008 | 5.007 |
| $^{37}ArCa/^{39}ArK$ | 9.315 | 6.818 | 7.202 | 14.086 | 13.499 | 15.062 | 20.973 | 11.417 | 9.035 | 9.695 | 7.306 | 6.135 | 13.077 | 8.819 | 8.744 |
| An | 50.092 | 46.801 | 48.686 | 55.995 | 56.368 | 60.082 | 65.151 | 54.437 | 51.107 | 52.294 | 48.428 | 46.470 | 55.461 | 48.894 | 51.034 |
| Ab | 46.969 | 49.448 | 47.620 | 41.833 | 41.351 | 37.738 | 33.152 | 42.957 | 45.802 | 44.759 | 47.950 | 49.391 | 42.222 | 48.077 | 45.777 |
| Or | 2.939 | 3.751 | 3.694 | 2.172 | 2.282 | 2.180 | 1.697 | 2.606 | 3.091 | 2.947 | 3.622 | 4.139 | 2.318 | 3.029 | 3.189 |

Table 1 (continued).

| Sample | TC992 | TC992 | TC992 | TC992 | TC992 | TC992 | TC992 | TC992 | TC992 | TC992 | TC992 | TC992 | TC-992 | TC-992 | TC-992 |
|---|---|---|---|---|---|---|---|---|---|---|---|---|---|---|---|
| **Analysis** | **124** | **128** | **129** | **131** | **132** | **134** | **135** | **138** | **140** | **141** | **142** | **144** | **15** | **16** | **19** |
| $SiO_2$ | 54.52 | 55.93 | 54.69 | 57.39 | 54.58 | 54.81 | 55.55 | 55.28 | 53.62 | 53.68 | 55.34 | 54.57 | 53.24 | 60.50 | 66.07 |
| $TiO_2$ | 0.05 | 0.07 | 0.04 | 0.05 | 0.04 | 0.03 | 0.05 | 0.05 | 0.04 | 0.05 | 0.05 | 0.04 | 0.03 | 0.15 | 0.02 |
| $Al_2O_3$ | 28.68 | 28.06 | 28.40 | 26.75 | 28.79 | 28.57 | 28.00 | 27.80 | 28.88 | 28.92 | 27.87 | 28.48 | 29.83 | 24.14 | 15.44 |
| $Cr_2O_3$ | 0.00 | 0.00 | 0.00 | 0.00 | 0.00 | 0.00 | 0.00 | 0.00 | 0.00 | 0.00 | 0.01 | 0.00 | | | |
| FeO | 0.42 | 0.55 | 0.46 | 0.43 | 0.38 | 0.41 | 0.56 | 0.51 | 0.50 | 0.53 | 0.56 | 0.52 | 0.75 | 0.85 | 2.61 |
| MnO | 0.00 | 0.00 | 0.00 | 0.01 | 0.00 | 0.01 | 0.00 | 0.01 | 0.01 | 0.02 | 0.02 | 0.01 | 0.02 | 0.00 | 0.06 |
| MgO | 0.06 | 0.05 | 0.04 | 0.06 | 0.06 | 0.04 | 0.06 | 0.06 | 0.06 | 0.08 | 0.08 | 0.06 | 0.12 | 0.00 | 1.56 |
| CaO | 11.31 | 10.46 | 11.15 | 9.08 | 11.36 | 11.21 | 10.45 | 10.64 | 11.79 | 11.80 | 10.65 | 11.27 | 12.85 | 6.44 | 0.88 |
| $Na_2O$ | 4.84 | 5.39 | 4.97 | 6.01 | 4.96 | 5.01 | 5.29 | 5.05 | 4.78 | 4.71 | 5.35 | 4.98 | 4.36 | 7.01 | 3.03 |
| $K_2O$ | 0.47 | 0.48 | 0.46 | 0.66 | 0.43 | 0.44 | 0.54 | 0.54 | 0.41 | 0.39 | 0.50 | 0.47 | 0.34 | 1.15 | 7.31 |
| Total | 100.35 | 100.99 | 100.21 | 100.46 | 100.60 | 100.52 | 100.51 | 99.95 | 100.08 | 100.19 | 100.42 | 100.39 | 101.54 | 100.24 | 96.98 |
| **Structural formulae to 8 oxygens** | | | | | | | | | | | | | | | |
| Si | 2.459 | 2.502 | 2.470 | 2.571 | 2.456 | 2.467 | 2.498 | 2.499 | 2.432 | 2.432 | 2.494 | 2.463 | 2.389 | 2.703 | 3.063 |
| Ti | 0.002 | 0.002 | 0.001 | 0.002 | 0.001 | 0.001 | 0.002 | 0.002 | 0.001 | 0.002 | 0.002 | 0.001 | 0.001 | 0.005 | 0.001 |
| Al | 1.525 | 1.479 | 1.512 | 1.412 | 1.527 | 1.516 | 1.484 | 1.481 | 1.544 | 1.544 | 1.480 | 1.515 | 1.577 | 1.271 | 0.844 |
| Cr | 0.000 | 0.000 | 0.000 | 0.000 | 0.000 | 0.000 | 0.000 | 0.000 | 0.000 | 0.000 | 0.000 | 0.000 | 0.000 | 0.000 | 0.000 |
| $Fe^{2+}$ | 0.016 | 0.021 | 0.017 | 0.016 | 0.014 | 0.015 | 0.021 | 0.019 | 0.019 | 0.020 | 0.021 | 0.020 | 0.028 | 0.032 | 0.101 |
| $Mn^{2+}$ | 0.000 | 0.000 | 0.000 | 0.000 | 0.000 | 0.000 | 0.000 | 0.000 | 0.000 | 0.001 | 0.001 | 0.000 | 0.001 | 0.000 | 0.002 |
| Mg | 0.004 | 0.003 | 0.003 | 0.004 | 0.004 | 0.003 | 0.004 | 0.004 | 0.004 | 0.005 | 0.005 | 0.004 | 0.008 | 0.000 | 0.108 |
| Ca | 0.547 | 0.501 | 0.540 | 0.436 | 0.548 | 0.541 | 0.504 | 0.515 | 0.573 | 0.573 | 0.514 | 0.545 | 0.618 | 0.308 | 0.044 |
| Na | 0.423 | 0.468 | 0.435 | 0.522 | 0.433 | 0.437 | 0.461 | 0.443 | 0.420 | 0.414 | 0.467 | 0.436 | 0.379 | 0.607 | 0.272 |
| K | 0.027 | 0.028 | 0.026 | 0.038 | 0.025 | 0.025 | 0.031 | 0.031 | 0.024 | 0.022 | 0.029 | 0.027 | 0.019 | 0.066 | 0.432 |
| Sum | 5.002 | 5.004 | 5.004 | 5.001 | 5.008 | 5.005 | 5.005 | 4.995 | 5.017 | 5.013 | 5.013 | 5.010 | 5.021 | 4.992 | 4.867 |
| $^{37}ArCa/^{39}ArK$ | 11.078 | 9.935 | 11.151 | 6.328 | 12.056 | 11.797 | 8.911 | 9.030 | 13.135 | 13.924 | 9.805 | 11.065 | 17.345 | 2.570 | 0.055 |
| An | 54.832 | 50.301 | 53.906 | 43.785 | 54.480 | 53.902 | 50.567 | 52.094 | 56.351 | 56.772 | 50.906 | 54.090 | 60.772 | 31.423 | 5.841 |
| Ab | 42.463 | 46.933 | 43.452 | 52.434 | 43.050 | 43.602 | 46.332 | 44.753 | 41.304 | 41.000 | 46.257 | 43.239 | 37.314 | 61.896 | 36.392 |
| Or | 2.705 | 2.766 | 2.642 | 3.781 | 2.469 | 2.497 | 3.101 | 3.152 | 2.344 | 2.228 | 2.837 | 2.671 | 1.915 | 6.681 | 57.768 |

Table 1 (continued).

| Sample | TC995A | TC995A | TC995A | TC995A | TC995A | TC995A | TC995A | TC995A | TC995A | TC995A | TC995A | TC995A | TC995A | TC995A | TC995A |
|---|---|---|---|---|---|---|---|---|---|---|---|---|---|---|---|
| **Analysis** | **31** | **32** | **33** | **34** | **35** | **36** | **37** | **38** | **42** | **43** | **48** | **49** | **52** | **1** | **2** |
| $SiO_2$ | 52.72 | 53.10 | 54.05 | 53.60 | 53.05 | 53.32 | 52.29 | 53.44 | 52.84 | 52.76 | 53.98 | 52.65 | 53.75 | 68.27 | 53.12 |
| $TiO_2$ | 0.06 | 0.04 | 0.05 | 0.05 | 0.05 | 0.04 | 0.05 | 0.05 | 0.05 | 0.05 | 0.06 | 0.07 | 0.06 | 0.01 | 0.08 |
| $Al_2O_3$ | 28.84 | 28.33 | 28.15 | 28.46 | 28.76 | 28.33 | 28.79 | 28.32 | 29.06 | 28.61 | 28.06 | 28.70 | 28.07 | 20.08 | 29.34 |
| $Cr_2O_3$ | 0.01 | 0.01 | 0.01 | 0.00 | 0.00 | 0.00 | 0.00 | 0.00 | 0.00 | 0.01 | 0.00 | 0.01 | 0.00 | | |
| FeO | 0.89 | 0.94 | 0.88 | 0.93 | 0.83 | 0.91 | 1.00 | 0.83 | 0.92 | 0.91 | 0.92 | 0.97 | 0.89 | 0.12 | 0.93 |
| MnO | 0.01 | 0.02 | 0.01 | 0.01 | 0.02 | 0.00 | 0.03 | 0.01 | 0.02 | 0.00 | 0.02 | 0.00 | 0.02 | 0.00 | 0.00 |
| MgO | 0.13 | 0.11 | 0.12 | 0.12 | 0.15 | 0.12 | 0.10 | 0.13 | 0.10 | 0.12 | 0.13 | 0.11 | 0.14 | 0.00 | 0.02 |
| CaO | 12.24 | 11.78 | 11.49 | 11.79 | 12.23 | 11.64 | 12.19 | 11.87 | 12.41 | 12.32 | 11.51 | 12.30 | 11.51 | 0.79 | 12.99 |
| $Na_2O$ | 4.15 | 4.46 | 4.65 | 4.51 | 4.15 | 4.52 | 4.34 | 4.42 | 4.18 | 4.21 | 4.57 | 4.32 | 4.61 | 10.92 | 4.00 |
| $K_2O$ | 0.55 | 0.46 | 0.68 | 0.62 | 0.50 | 0.54 | 0.45 | 0.62 | 0.52 | 0.54 | 0.66 | 0.51 | 0.65 | 0.10 | 0.45 |
| Total | 99.61 | 99.26 | 100.09 | 100.08 | 99.74 | 99.43 | 99.23 | 99.68 | 100.12 | 99.52 | 99.91 | 99.64 | 99.70 | 100.29 | 100.93 |
| **Structural formulae to 8 oxygens** | | | | | | | | | | | | | | | |
| Si | 2.411 | 2.433 | 2.455 | 2.437 | 2.420 | 2.438 | 2.402 | 2.439 | 2.405 | 2.415 | 2.456 | 2.409 | 2.452 | 2.974 | 2.399 |
| Ti | 0.002 | 0.001 | 0.002 | 0.002 | 0.002 | 0.001 | 0.002 | 0.002 | 0.002 | 0.002 | 0.002 | 0.002 | 0.002 | 0.000 | 0.003 |
| Al | 1.554 | 1.530 | 1.507 | 1.525 | 1.546 | 1.527 | 1.559 | 1.523 | 1.559 | 1.544 | 1.505 | 1.548 | 1.509 | 1.031 | 1.562 |
| Cr | 0.000 | 0.000 | 0.000 | 0.000 | 0.000 | 0.000 | 0.000 | 0.000 | 0.000 | 0.000 | 0.000 | 0.000 | 0.000 | 0.000 | 0.000 |
| $Fe^{2+}$ | 0.034 | 0.036 | 0.033 | 0.035 | 0.032 | 0.035 | 0.039 | 0.032 | 0.035 | 0.035 | 0.035 | 0.037 | 0.034 | 0.004 | 0.035 |
| $Mn^{2+}$ | 0.000 | 0.001 | 0.000 | 0.000 | 0.001 | 0.000 | 0.001 | 0.000 | 0.001 | 0.000 | 0.001 | 0.000 | 0.001 | 0.000 | 0.000 |
| Mg | 0.009 | 0.008 | 0.008 | 0.008 | 0.010 | 0.008 | 0.007 | 0.009 | 0.007 | 0.008 | 0.009 | 0.007 | 0.010 | 0.000 | 0.001 |
| Ca | 0.600 | 0.578 | 0.559 | 0.574 | 0.597 | 0.570 | 0.600 | 0.580 | 0.605 | 0.604 | 0.561 | 0.603 | 0.562 | 0.037 | 0.629 |
| Na | 0.368 | 0.396 | 0.409 | 0.398 | 0.367 | 0.401 | 0.387 | 0.391 | 0.369 | 0.373 | 0.403 | 0.383 | 0.408 | 0.922 | 0.350 |
| K | 0.032 | 0.027 | 0.040 | 0.036 | 0.029 | 0.031 | 0.026 | 0.036 | 0.030 | 0.032 | 0.038 | 0.030 | 0.038 | 0.006 | 0.026 |
| Sum | 5.010 | 5.012 | 5.014 | 5.015 | 5.004 | 5.013 | 5.023 | 5.011 | 5.013 | 5.013 | 5.010 | 5.021 | 5.015 | 4.974 | 5.005 |
| $^{37}ArCa/^{39}ArK$ | 10.137 | 11.627 | 7.704 | 8.737 | 11.117 | 9.964 | 12.414 | 8.761 | 10.872 | 10.404 | 7.985 | 11.135 | 8.164 | 3.626 | 13.248 |
| An | 59.955 | 57.723 | 55.470 | 56.976 | 60.094 | 56.896 | 59.223 | 57.604 | 60.240 | 59.855 | 55.938 | 59.359 | 55.806 | 3.822 | 62.559 |
| Ab | 36.813 | 39.565 | 40.595 | 39.461 | 36.952 | 39.984 | 38.170 | 38.804 | 36.732 | 37.001 | 40.235 | 37.728 | 40.459 | 95.602 | 34.860 |
| Or | 3.232 | 2.713 | 3.934 | 3.563 | 2.954 | 3.120 | 2.607 | 3.593 | 3.028 | 3.144 | 3.828 | 2.913 | 3.735 | 0.576 | 2.580 |

**TABLE 2. MICROPROBE ANALYSES OF CLINOPYROXENES.**

| Samlpe | TC995A | TC995A | TC995A | TC995A | TC995A | TC995A | TC995A | TC995A | TC995A | TC995A | TC995A |
|---|---|---|---|---|---|---|---|---|---|---|---|
| **Analysis** | **39** | **40** | **41** | **44** | **46** | **47** | **50** | **51** | **53** | **4** | **5** |
| $SiO_2$ | 51.36 | 51.39 | 51.35 | 51.12 | 51.09 | 51.30 | 50.40 | 51.01 | 51.13 | 49.75 | 51.91 |
| $TiO_2$ | 0.54 | 0.58 | 0.56 | 0.56 | 0.57 | 0.55 | 0.56 | 0.55 | 0.56 | 0.97 | 0.72 |
| $Al_2O_3$ | 2.21 | 2.31 | 1.95 | 2.10 | 2.24 | 2.22 | 2.17 | 1.98 | 1.97 | 3.89 | 2.22 |
| $Cr_2O_3$ | 0.02 | 0.01 | 0.00 | 0.00 | 0.03 | 0.01 | 0.03 | 0.01 | 0.00 | | |
| FeO | 11.03 | 10.91 | 11.30 | 11.24 | 11.33 | 10.69 | 11.27 | 11.08 | 11.03 | 13.55 | 12.18 |
| MnO | 0.39 | 0.39 | 0.44 | 0.38 | 0.37 | 0.38 | 0.40 | 0.38 | 0.42 | 0.39 | 0.35 |
| MgO | 15.76 | 15.72 | 15.49 | 15.90 | 15.47 | 15.92 | 15.41 | 15.62 | 15.64 | 13.38 | 14.69 |
| CaO | 18.12 | 18.12 | 18.26 | 17.95 | 18.06 | 18.21 | 17.97 | 18.33 | 18.23 | 18.40 | 18.57 |
| $Na_2O$ | 0.32 | 0.31 | 0.32 | 0.34 | 0.30 | 0.23 | 0.29 | 0.28 | 0.28 | 0.40 | 0.39 |
| $K_2O$ | 0.00 | 0.00 | 0.00 | 0.00 | 0.00 | 0.00 | 0.00 | 0.00 | 0.01 | 0.02 | 0.02 |
| NiO | 0.00 | 0.03 | 0.01 | 0.03 | 0.01 | 0.00 | 0.00 | 0.03 | 0.03 | | |
| Sum | 99.76 | 99.77 | 99.68 | 99.62 | 99.46 | 99.52 | 98.50 | 99.25 | 99.30 | 100.75 | 101.05 |
| **Structural formulae to 6 oxygens** | | | | | | | | | | | |
| Si | 1.911 | 1.912 | 1.917 | 1.905 | 1.910 | 1.912 | 1.903 | 1.910 | 1.914 | 1.857 | 1.920 |
| $Al^{iv}$ | 0.089 | 0.088 | 0.083 | 0.092 | 0.090 | 0.088 | 0.097 | 0.087 | 0.086 | 0.143 | 0.080 |
| Ti | 0.015 | 0.016 | 0.016 | 0.016 | 0.016 | 0.015 | 0.016 | 0.015 | 0.016 | 0.027 | 0.020 |
| $Al^{vi}$ | 0.008 | 0.013 | 0.002 | 0.000 | 0.009 | 0.010 | 0.000 | 0.000 | 0.001 | 0.028 | 0.017 |
| $Fe^{3+}$ | 0.073 | 0.065 | 0.072 | 0.092 | 0.070 | 0.064 | 0.086 | 0.082 | 0.076 | 0.091 | 0.051 |
| Cr | 0.001 | 0.000 | 0.000 | 0.000 | 0.001 | 0.000 | 0.001 | 0.000 | 0.000 | 0.000 | 0.000 |
| $Fe^{2+}$ | 0.273 | 0.277 | 0.282 | 0.261 | 0.287 | 0.271 | 0.272 | 0.267 | 0.272 | 0.335 | 0.327 |
| $Mn^{2+}$ | 0.012 | 0.012 | 0.014 | 0.012 | 0.012 | 0.012 | 0.013 | 0.012 | 0.013 | 0.012 | 0.011 |
| Mg | 0.874 | 0.872 | 0.862 | 0.883 | 0.863 | 0.885 | 0.867 | 0.872 | 0.872 | 0.744 | 0.810 |
| Ca | 0.723 | 0.722 | 0.730 | 0.717 | 0.724 | 0.727 | 0.727 | 0.735 | 0.731 | 0.736 | 0.736 |
| Na | 0.023 | 0.023 | 0.023 | 0.024 | 0.022 | 0.017 | 0.021 | 0.020 | 0.021 | 0.029 | 0.028 |
| K | 0.000 | 0.000 | 0.000 | 0.000 | 0.000 | 0.000 | 0.000 | 0.000 | 0.001 | 0.001 | 0.001 |
| Ni | 0.000 | 0.001 | 0.000 | 0.001 | 0.000 | 0.000 | 0.000 | 0.001 | 0.001 | 0.000 | 0.000 |
| Sum cat. | 4.002 | 4.002 | 4.002 | 4.003 | 4.002 | 4.002 | 4.003 | 4.002 | 4.002 | 4.003 | 4.002 |
| [mg] | 0.762 | 0.759 | 0.753 | 0.772 | 0.750 | 0.766 | 0.761 | 0.765 | 0.763 | 0.690 | 0.712 |
| En | 44.725 | 44.765 | 43.959 | 44.955 | 44.141 | 45.163 | 44.137 | 44.286 | 44.419 | 38.799 | 41.855 |
| Fs | 18.304 | 18.159 | 18.808 | 18.572 | 18.836 | 17.710 | 18.881 | 18.355 | 18.366 | 22.854 | 20.118 |
| Wo | 36.971 | 37.075 | 37.233 | 36.473 | 37.023 | 37.127 | 36.982 | 37.358 | 37.215 | 38.347 | 38.027 |

a maximum flux gradient estimated at ±0.2% (1σ) in the volume containing the samples. The Hb3Gr hornblende and the Fish Canyon sanidine FCs, with an age of 1072 Ma (Turner *et al*., 1971; Renne *et al*., 1998; Jourdan *et al*., 2006) and 28.02 Ma (Renne *et al.*, 1998), respectively, were used as flux monitors. Two distinct $^{40}Ar/^{39}Ar$ dating methods have been carried out. Populations of *ca.* 30 to 43 mg fraction, 200-315 μm in size, were measured with a double vacuum high frequency heater, whereas clusters (10 to 80) of grains, 200-315 and 315-500 μm in size, were heated with a laser. Argon analyses were carried out in the geochronological laboratory of the Université de Nice-Sophia Antipolis (Nice, France).

The plagioclase bulk samples were step heated in a high frequency furnace, connected to a 120°/12 cm M.A.S.S.E. mass spectrometer working with a Baür-Signer GS 98 source and a Balzers SEV 217 electron multiplier. For small clusters of plagioclase grains, gas extraction was carried out with a $CO_2$ Synrad 48-5 continuous laser; the mass spectrometer is a VG 3600 working with a Daly detector system. The typical blank values for the extraction and purification laser system, which are currently measured every third step, were in the range $1.4\text{-}10\text{-}x10^{-13}$ ccSTP for $^{40}Ar$, $0.4\text{-}4.5x10^{-14}$ ccSTP for $^{39}Ar$, $0.7\text{-}1.4x10^{-13}$ ccSTP for $^{37}Ar$, and $2\text{-}3x10^{-14}$ ccSTP for $^{36}Ar$. The criteria for defining plateau ages were

the following: **1.** it should contain at least 70% of released $^{39}Ar$, **2.** there should be at least three successive steps in the plateau and **3.** the integrated age of the plateau should agree with each apparent age of the plateau within a 2σ error confidence interval. Uncertainties on the apparent ages on each step do not include the errors on the $^{40}Ar^*/^{39}Ar_K$ ratio and the age of the monitor. Errors on plateau and isochron ages are given at the 2σ level. The error on the $^{40}Ar^*/^{39}Ar_K$ ratio of the monitor is included in the plateau age error bar calculation, but not the error on the age of the monitor and the decay constants. $^{40}Ar/^{39}Ar$ analytical results are given in table 3.

Sr and Nd isotopic data (Table 4) were obtained on plagioclase, clinopyroxenes and whole-rock of sample TC99-5a (sector B, Fig. 1) at the 'Centro de Instrumentación Científica, Universidad de Granada, España', using a Finnigan MAT 262 thermal ionization mass spectrometer (TIMS) with variable multicollector and RPQ. Normalization value for $^{87}Sr/^{86}Sr$ was $^{88}Sr/^{86}Sr$=8.375209 and the reproductibility under successive determinations of the NBS-987 dissolved standard were better than 0.0007% (2σ). For the Nd determinations, the normalization value for $^{143}Nd/^{144}Nd$ was $^{146}Nd/^{144}Nd$=0.7219, with a precision better than 0.0016% (2σ) calculated under successive measures of the WSE power standard. The reproductibility under successive measures of the La Jolla dissolution standard was better than 0.0014% (2σ). Rb/Sr and Sm/Nd isochrones were calculated using the ISOPLOT 2.45 software (Ludwig, 2000). Elemental Rb, Sr, Sm and Nd contents were analysed by inductively coupled plasma mass spectrometry (ICP-MS, Perkin-Elmer Sciex Elan 5000, 'Centro de Instrumentación Científica, Universidad de Granada, España').

**TABLE 3. $^{40}Ar/^{39}Ar$ ANALYTICAL RESULTS OBTAINED ON PRIMARY PLAGIOCLASE FROM THE LOWER CRETACEOUS VOLCANIC ROCKS IN THE COASTAL RANGE OF LA SERENA REGION (30°S). ERROR BARS ARE GIVEN AT THE 1σ LEVEL.**

| Temp. (°C) or step nb | Atmospheric contamination (%) | $^{39}Ar$ (%) | $^{37}Ar_{Ca}/^{39}Ar_K$ | $^{40}Ar^*/^{39}Ar_K$ | Apparent age (Ma±1σ) |
|---|---|---|---|---|---|
| **ARQ99.4 plagioclase (M1356), 30 mg (furnace heating) (J=0.01760±0.00007)** | | | | | |
| 550 | 100 | 0.00 | 3.446 | - | - ± - |
| 650 | 92.4 | 0.23 | 3.852 | 2.839 | 88.01 ± 11.56 |
| 700 | 78.0 | 0.33 | 4.950 | 3.679 | 113.24 ± 7.92 |
| 750 | 69.7 | 1.88 | 5.964 | 3.567 | 109.89 ± 2.09 |
| 800 | 20.0 | 3.98 | 6.544 | 3.698 | 113.80 ± 0.78 |
| 850 | 11.4 | 4.30 | 6.681 | 3.680 | 113.25 ± 0.67 |
| 900 | 12.3 | 9.58 | 6.582 | 3.659 | 112.64 ± 0.35 |
| 950 | 11.0 | 8.85 | 5.971 | 3.533 | 108.87 ± 0.41 |
| 1000 | 9.0 | 11.41 | 6.100 | 3.570 | 109.97 ± 0.39 |
| 1050 | 15.5 | 8.72 | 5.454 | 3.431 | 105.81 ± 0.41 |
| 1100 | 25.3 | 5.96 | 5.768 | 3.485 | 107.44 ± 0.60 |
| 1150 | 28.6 | 5.03 | 6.090 | 3.567 | 109.90 ± 0.60 |
| 1200 | 28.3 | 3.98 | 6.417 | 3.638 | 112.00 ± 0.82 |
| 1250 | 20.9 | 5.00 | 6.599 | 3.689 | 113.53 ± 0.70 |
| 1300 | 16.7 | 3.41 | 6.736 | 3.719 | 114.44 ± 0.77 |
| 1350 | 15.5 | 5.72 | 6.753 | 3.698 | 113.80 ± 0.50 |
| 1400 | 14.8 | 15.31 | 6.801 | 3.733 | 114.83 ± 0.42 |
| 1450 | 17.7 | 5.52 | 6.792 | 3.740 | 115.05 ± 0.63 |
| fuse | 15.9 | 0.76 | 6.776 | 3.633 | 111.87 ± 1.93 |
| | | | | | Integrated age = 111.5 ± 0.1 Ma |
| **ARQ99.4 plagioclase (G530), 10 grains (laser heating) (J=0.01764±0.00007)** | | | | | |
| 1 | 25.4 | 3.37 | 6.357 | 3.725 | 114.84 ± 1.45 |
| 2 | 6.6 | 8.31 | 6.504 | 3.624 | 111.81 ± 0.85 |
| 3 | 4.5 | 6.19 | 6.613 | 3.626 | 111.88 ± 1.14 |
| 4 | 2.2 | 7.82 | 6.593 | 3.662 | 112.94 ± 0.69 |
| 5 | 2.0 | 9.66 | 6.602 | 3.694 | 113.90 ± 0.74 |
| 6 | 4.1 | 8.37 | 6.560 | 3.806 | 117.26 ± 1.33 |
| 7 | 4.2 | 13.92 | 6.466 | 3.692 | 113.85 ± 0.58 |
| 8 | 2.6 | 7.27 | 6.591 | 3.696 | 113.98 ± 0.90 |
| 9 | 2.8 | 18.12 | 6.656 | 3.687 | 113.70 ± 0.54 |
| fuse | 1.9 | 16.97 | 6.834 | 3.692 | 113.84 ± 0.44 |
| | | | | | Integrated age = 113.8 ± 0.2 Ma |

Table 3 (continued).

| Temp. (°C) or step nb | Atmospheric contamination (%) | $^{39}Ar$ (%) | $^{37}Ar_{Ca}/^{39}Ar_{K}$ | $^{40}Ar^{*}/^{39}Ar_{K}$ | Apparent age (Ma±1σ) |
|---|---|---|---|---|---|
| **ARQ99.7 plagioclase (M1353), 25 mg (furnace heating) (J = 0.01760 ± 0.00007)** | | | | | |
| 550 | 99.7 | 0.05 | 1.687 | 0.266 | 8.43 ± 44.69 |
| 650 | 90.8 | 0.67 | 1.946 | 2.158 | 67.26 ± 7.59 |
| 700 | 79.4 | 1.04 | 2.768 | 2.248 | 70.02 ± 3.70 |
| 750 | 85.7 | 2.45 | 3.952 | 2.227 | 69.36 ± 3.08 |
| 800 | 45.4 | 3.89 | 7.474 | 2.651 | 82.27 ± 1.11 |
| 830 | 26.8 | 2.72 | 8.597 | 2.598 | 80.68 ± 0.93 |
| 870 | 40.2 | 6.31 | 8.462 | 2.576 | 80.01 ± 0.70 |
| 920 | 32.3 | 9.51 | 5.175 | 2.465 | 76.64 ± 0.62 |
| 970 | 29.0 | 9.91 | 5.382 | 2.467 | 76.69 ± 0.47 |
| 1020 | 30.9 | 15.28 | 3.520 | 2.406 | 74.82 ± 0.38 |
| 1070 | 42.2 | 9.34 | 3.799 | 2.367 | 73.64 ± 0.75 |
| 1120 | 55.9 | 6.30 | 4.603 | 2.339 | 72.80 ± 0.83 |
| 1170 | 58.4 | 7.52 | 5.207 | 2.410 | 74.96 ± 1.11 |
| 1220 | 57.6 | 4.82 | 6.172 | 2.460 | 76.47 ± 0.97 |
| 1270 | 55.7 | 2.91 | 7.245 | 2.541 | 78.95 ± 1.64 |
| 1320 | 53.3 | 2.95 | 8.858 | 2.583 | 80.23 ± 1.51 |
| 1370 | 48.9 | 3.42 | 10.501 | 2.669 | 82.83 ± 1.38 |
| 1420 | 49.3 | 7.51 | 11.389 | 2.716 | 84.26 ± 1.00 |
| 1470 | 42.3 | 3.25 | 12.317 | 2.757 | 85.51 ± 1.06 |
| fuse | 47.9 | 0.15 | 12.164 | 2.140 | 66.71 ± 11.94 |
| | | | | | Integrated age = 77.1 ± 0.2 Ma |
| **ARQ99.7 plagioclase (H109), (laser heating) (J = 0.01745 ± 0.00007)** | | | | | |
| 1 | 86.9 | 3.82 | 5.972 | 2.362 | 72.88 ± 3.24 |
| 2 | 50.2 | 1.85 | 8.563 | 2.485 | 76.61 ± 3.05 |
| 3 | 46.7 | 2.43 | 8.987 | 2.545 | 78.40 ± 2.31 |
| 4 | 43.2 | 5.66 | 8.012 | 2.514 | 77.49 ± 1.86 |
| 5 | 33.3 | 4.61 | 7.962 | 2.544 | 78.38 ± 1.60 |
| 6 | 36.5 | 6.05 | 7.834 | 2.451 | 75.57 ± 1.19 |
| 7 | 33.8 | 7.38 | 8.435 | 2.489 | 76.70 ± 1.51 |
| 8 | 25.9 | 5.12 | 8.810 | 2.563 | 78.96 ± 1.28 |
| 9 | 34.6 | 6.64 | 8.750 | 2.503 | 77.15 ± 0.96 |
| 10 | 37.0 | 8.89 | 9.883 | 2.551 | 78.59 ± 0.71 |
| 11 | 37.2 | 6.41 | 9.950 | 2.572 | 79.21 ± 0.75 |
| 12 | 38.0 | 7.27 | 10.860 | 2.573 | 79.25 ± 1.05 |
| 13 | 29.8 | 4.60 | 11.811 | 2.677 | 82.39 ± 1.46 |
| 14 | 30.6 | 9.16 | 12.023 | 2.675 | 82.31 ± 1.17 |
| fuse | 33.3 | 20.10 | 12.809 | 2.700 | 83.08 ± 0.64 |
| | | | | | Integrated age = 79.4 ± 0.3 Ma |
| **ARQ99.7 plagioclase (G543), 15 grains (laser heating) (J = 0.01764 ± 0.00007)** | | | | | |
| 1 | 58.8 | 3.69 | 12.408 | 3.042 | 94.31 ± 7.51 |
| 2 | 13.5 | 1.73 | 13.250 | 2.754 | 85.61 ± 11.79 |
| 3 | 14.7 | 16.34 | 13.138 | 2.675 | 83.19 ± 1.84 |
| 4 | 10.5 | 21.59 | 13.578 | 2.678 | 83.27 ± 1.32 |
| 5 | 16.1 | 18.69 | 13.417 | 2.705 | 84.12 ± 1.46 |
| fuse | 9.7 | 37.96 | 13.834 | 2.751 | 85.51 ± 0.93 |
| | | | | | Integrated age = 84.7 ± 0.7 Ma |
| **TC99.5A plagioclase (M1354), 43 mg (furnace heating) (J = 0.01758 ± 0.00007)** | | | | | |
| 550 | 73.7 | 0.00 | 1.229 | 20.229 | 549.26 ± 910.53 |
| 650 | 89.0 | 0.21 | 4.775 | 4.409 | 134.77 ± 13.21 |
| 700 | 68.2 | 0.37 | 8.482 | 3.766 | 115.73 ± 6.17 |
| 750 | 49.1 | 0.85 | 8.362 | 3.521 | 108.43 ± 2.22 |
| 800 | 19.2 | 2.79 | 8.559 | 3.508 | 108.04 ± 0.81 |
| 850 | 8.9 | 4.77 | 8.584 | 3.549 | 109.27 ± 0.53 |
| 900 | 5.5 | 8.21 | 8.587 | 3.586 | 110.37 ± 0.42 |
| 950 | 3.2 | 7.22 | 8.556 | 3.652 | 112.34 ± 0.46 |
| 1000 | 3.6 | 11.71 | 8.530 | 3.652 | 112.33 ± 0.41 |
| 1050 | 2.4 | 9.06 | 8.498 | 3.680 | 113.16 ± 0.40 |
| 1100 | 5.2 | 6.52 | 8.419 | 3.689 | 113.44 ± 0.38 |
| 1150 | 6.4 | 5.67 | 8.494 | 3.818 | 117.28 ± 0.46 |
| 1200 | 7.1 | 6.35 | 8.544 | 3.868 | 118.79 ± 0.50 |
| 1250 | 6.8 | 4.50 | 8.549 | 3.840 | 117.95 ± 0.77 |
| 1300 | 6.2 | 3.46 | 8.533 | 3.803 | 116.83 ± 0.67 |
| 1350 | 5.4 | 9.31 | 8.506 | 3.804 | 116.87 ± 0.40 |
| 1400 | 5.8 | 8.24 | 8.517 | 3.795 | 116.59 ± 0.45 |
| 1450 | 6.1 | 10.10 | 8.514 | 3.811 | 117.08 ± 0.42 |
| Fuse | 6.3 | 0.65 | 8.548 | 3.706 | 113.97 ± 2.40 |
| | | | | | Integrated age = 114.5 ± 0.1 Ma |

Table 3 (continued).

| Temp. (°C) or step nb | Atmospheric contamination (%) | $^{39}Ar$ (%) | $^{37}Ar_{Ca}/^{39}Ar_{K}$ | $^{40}Ar^{*}/^{39}Ar_{K}$ | Apparent age (Ma ± 1σ) |
|---|---|---|---|---|---|
| **TC99.5A plagioclase (H44), 80 grains (laser heating) (J = 0.017454 ± 0.00007)** | | | | | |
| 1 | 53.0 | 0.87 | 6.934 | 5.990 | 179.39 ± 6.03 |
| 2 | 25.7 | 0.89 | 7.619 | 3.696 | 112.78 ± 4.82 |
| 3 | 17.8 | 1.34 | 8.028 | 3.537 | 108.08 ± 3.20 |
| 4 | 8.5 | 2.73 | 8.295 | 3.729 | 113.75 ± 1.94 |
| 5 | 4.8 | 4.29 | 8.426 | 3.722 | 113.54 ± 1.47 |
| 6 | 3.7 | 5.91 | 8.504 | 3.671 | 112.05 ± 1.16 |
| 7 | 3.3 | 9.23 | 8.512 | 3.646 | 111.31 ± 0.73 |
| 8 | 3.5 | 6.28 | 8.548 | 3.645 | 111.27 ± 0.86 |
| 9 | 4.9 | 5.90 | 8.531 | 3.648 | 111.37 ± 0.84 |
| 10 | 3.8 | 6.16 | 8.593 | 3.693 | 112.70 ± 0.96 |
| 11 | 3.4 | 7.66 | 8.531 | 3.782 | 115.32 ± 0.66 |
| 12 | 2.7 | 5.18 | 8.557 | 3.800 | 115.84 ± 0.86 |
| 13 | 4.0 | 4.12 | 8.536 | 3.790 | 115.56 ± 1.06 |
| 14 | 4.3 | 9.81 | 8.455 | 3.783 | 115.35 ± 0.73 |
| 15 | 3.5 | 12.22 | 8.421 | 3.767 | 114.87 ± 0.55 |
| 16 | 2.4 | 10.19 | 8.492 | 3.784 | 115.39 ± 0.57 |
| fuse | 4.0 | 7.19 | 8.600 | 3.771 | 114.98 ± 0.80 |
| | | | | | Integrated age = 114.4 ± 0.2 Ma |
| **TC99.2 plagioclase (M1355), 37 mg (furnace heating) (J = 0.01758 ± 0.00007)** | | | | | |
| 550 | 94.1 | 0.00 | 1.607 | 4.635 | 141.42 ± 359.18 |
| 650 | 89.8 | 0.48 | 2.303 | 1.929 | 60.22 ± 5.27 |
| 700 | 68.2 | 1.03 | 3.612 | 2.537 | 78.78 ± 2.69 |
| 750 | 61.0 | 1.64 | 3.883 | 2.812 | 87.14 ± 1.95 |
| 800 | 36.8 | 3.03 | 5.599 | 2.906 | 89.97 ± 0.84 |
| 850 | 19.3 | 6.16 | 6.945 | 2.942 | 91.05 ± 0.53 |
| 900 | 18.1 | 12.88 | 5.740 | 2.900 | 89.77 ± 0.35 |
| 950 | 13.4 | 8.88 | 5.802 | 2.885 | 89.33 ± 0.35 |
| 1000 | 13.2 | 14.81 | 4.570 | 2.879 | 89.13 ± 0.34 |
| 1050 | 15.8 | 9.04 | 4.259 | 2.836 | 87.86 ± 0.34 |
| 1100 | 22.0 | 5.66 | 4.568 | 2.832 | 87.74 ± 0.40 |
| 1150 | 27.9 | 8.79 | 4.727 | 2.856 | 88.46 ± 0.45 |
| 1200 | 24.3 | 2.53 | 6.644 | 2.920 | 90.39 ± 0.82 |
| 1250 | 25.3 | 4.17 | 6.997 | 2.930 | 90.70 ± 0.77 |
| 1300 | 21.4 | 2.30 | 7.519 | 2.931 | 90.72 ± 1.01 |
| 1350 | 21.0 | 6.73 | 7.647 | 2.970 | 91.88 ± 0.51 |
| 1400 | 23.5 | 7.02 | 8.017 | 2.976 | 92.08 ± 0.62 |
| 1450 | 22.7 | 4.55 | 8.622 | 3.011 | 93.12 ± 0.75 |
| fuse | 25.202 | 0.31 | 8.423 | 2.797 | 86.670 ± 4.676 |
| | | | | | Integrated age = 89.6 ± 0.1 Ma |
| **TC99.2 plagioclase (G540), 13 grains (laser heating) (J = 0.01764 ± 0.00007)** | | | | | |
| 1 | 8.4 | 1.40 | 6.650 | 3.110 | 96.38 ± 6.31 |
| 2 | 15.2 | 1.21 | 7.279 | 2.792 | 86.74 ± 5.79 |
| 3 | 9.3 | 3.93 | 7.344 | 2.853 | 88.59 ± 1.83 |
| 4 | 4.1 | 9.94 | 7.654 | 2.938 | 91.17 ± 0.77 |
| 5 | 4.3 | 9.20 | 7.842 | 2.943 | 91.33 ± 0.88 |
| 6 | 5.5 | 13.55 | 8.216 | 2.919 | 90.59 ± 0.93 |
| 7 | 5.4 | 14.46 | 8.126 | 2.929 | 90.80 ± 0.65 |
| 8 | 5.9 | 12.46 | 8.030 | 2.923 | 90.71 ± 0.69 |
| Fuse | 5.3 | 33.86 | 8.658 | 2.938 | 91.16 ± 0.46 |
| | | | | | Integrated age = 90.9 ± 0.3 Ma |

**TABLE 4. Sr-Nd ISOTOPIC DATA FOR THE LAVAS OF THE EARLY CRETACEOUS FROM THE COASTAL RANGE IN LA SERENA REGION (30ºS).**

| | Type | $SiO_2$ (%) | Rb (ppm) | Sr (ppm) | Sm (ppm) | Nd (ppm) | $^{87}Rb/^{86}Sr$ | $^{87}Sr/^{86}Sr$ | 2σ% | $^{147}Sm/^{144}Nd$ | $^{143}Nd/^{144}Nd$ | 2σ% |
|---|---|---|---|---|---|---|---|---|---|---|---|---|
| TC99-5a | β–α | 52.2 | 78.55 | 502.7 | 5.620 | 25.133 | 0.4520 | 0.70437 | 0.003 | 0.1353 | 0.512750 | 0.001 |
| TC99-5a(pl) | Pl | 50.0 | 4.13 | 1195.5 | 0.414 | 3.212 | 0.0100 | 0.70358 | 0.003 | 0.0780 | 0.512726 | 0.003 |
| TC99-5a(px) | Cpx | 50.0 | 2.14 | 21.6 | 6.093 | 18.049 | 0.2863 | 0.70399 | 0.003 | 0.2042 | 0.512822 | 0.002 |

β-α**:** basaltic andesite; **Pl:** plagioclase; **Cpx:** clinopyroxene.

## 4. Petrology and Mineral Chemistry

The four analysed samples are porphyritic to highly porphyritic (20-30% phenocrysts) basaltic andesites with large (up to 2-3 cm), mostly unzoned, plagioclase phenocrysts (*ca*. 80% of the total phenocrysts) and up to 1 cm clinopyroxenes. Minor idiomorphic olivine, always pseudomorphosed by iron oxide and mafic phyllosilicates, and small idiomorphic magnetite and Ti-magnetite are also found as phenocrysts. Microcrystalline plagioclase, augite, and magnetite make up the intergranular to cryptocrystalline groundmass (Morata and Aguirre, 2003). Minor sericite in plagioclase phenocrysts is the main secondary mineral. Sample ARQ99-7 is a dyke with petrographical and mineralogical characteristics similar to those of the lavas.

Plagioclase phenocrysts from samples ARQ99-4, ARQ99-7 and TC99-5a have a rather homogeneous composition (Table 1 and Fig. 2), ranging from $An_{62}Ab_{35}Or_3$ at the core to $An_{55}Ab_{41}Or_4$ at the rims. Nevertheless, a strong zoning is observed in plagioclases from sample TC99-2, ranging in composition from $An_{65}Ab_{33}Or_2$ to $An_{44}Ab_{52}Or_4$. Differences between plagioclase from sample TC99-2 and the other three dated rocks are also observed in the $Fe^{2+}$ and K contents (Fig. 3) and could be the consequence of differences in the redox conditions in parental magmas from which the lavas were generated *(e.g*., Tegner, 1997).

SEM images of samples ARQ99-4 and ARQ99-7 (Fig. 4) allow the identification of patches of ≈200-300 μ of fresh plagioclase, whereas plagioclase from sample TC99-5a is characterized by a weaker alteration degree (Fig. 5a) with a relatively high chemical homogeneity from core to rim (Figs. 5b and c).

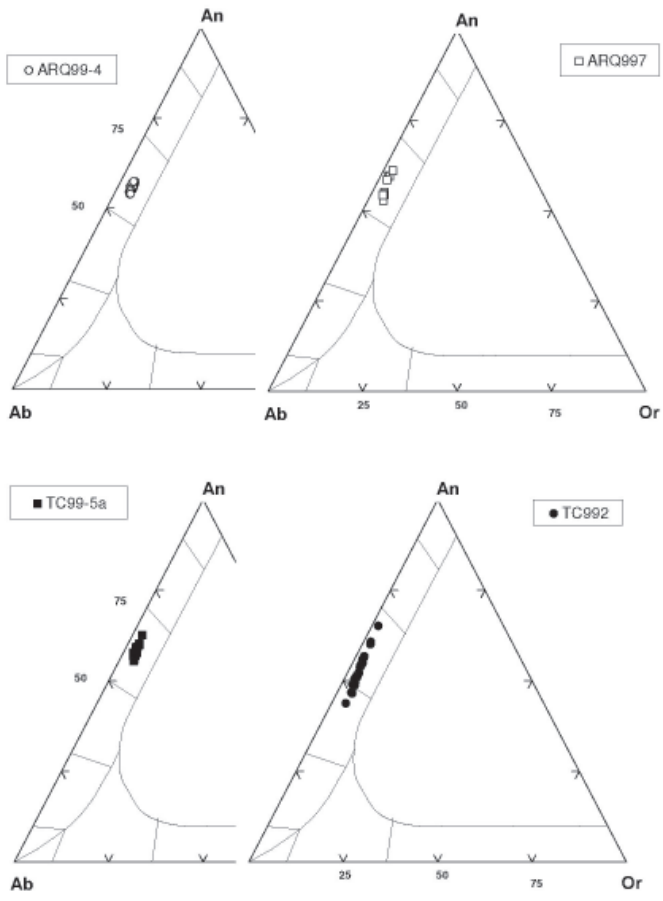


FIG. 2. Chemical variations on an An-Ab-Or diagram for the primary plagioclase chemistry of the Lower Cretaceous volcanic rocks from La Serena area. Samples ARQ99-4 and ARQ99-7 from area A in figure 1 and samples TC99-2 and TC99-5a from area B in figure 1.

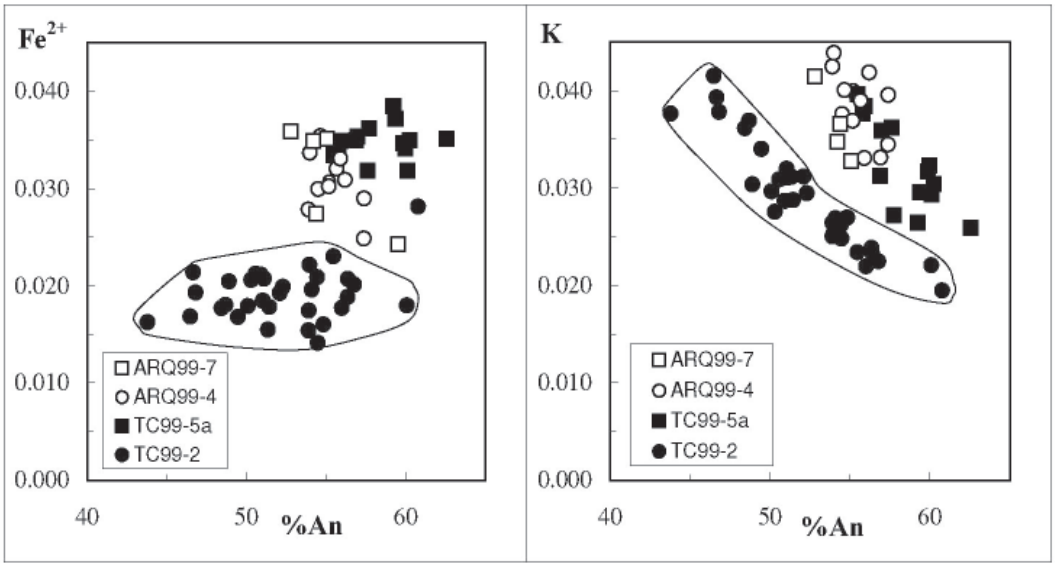


FIG. 3. %An *versus* $Fe^{2+}$ (a.p.f.u.) diagram and An *versus* K (a.p.f.u.) diagram for dated plagioclase. Symbols as in figure 2.

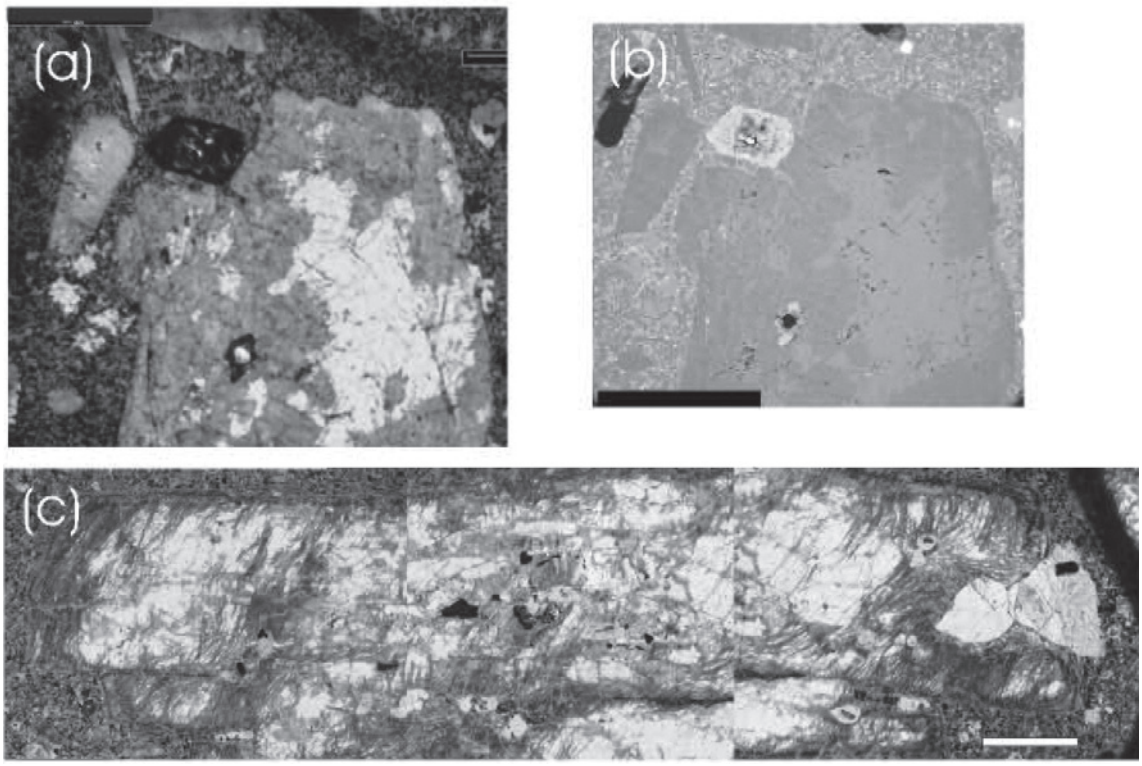


FIG. 4. **a.** Microscope photograph of a plagioclase phenocryst from sample ARQ99-4. Scale bar: 0.5 mm; **b.** Scanning electron micrograph (back-scattered electron image) showing core free of alteration and rims wholly sericiticed. Scale bar: 3 mm; **c.** Microscope photograph of a plagioclase phenocryst from sample ARQ997 showing areas free of alteration. Scale bar: 0.5 mm.

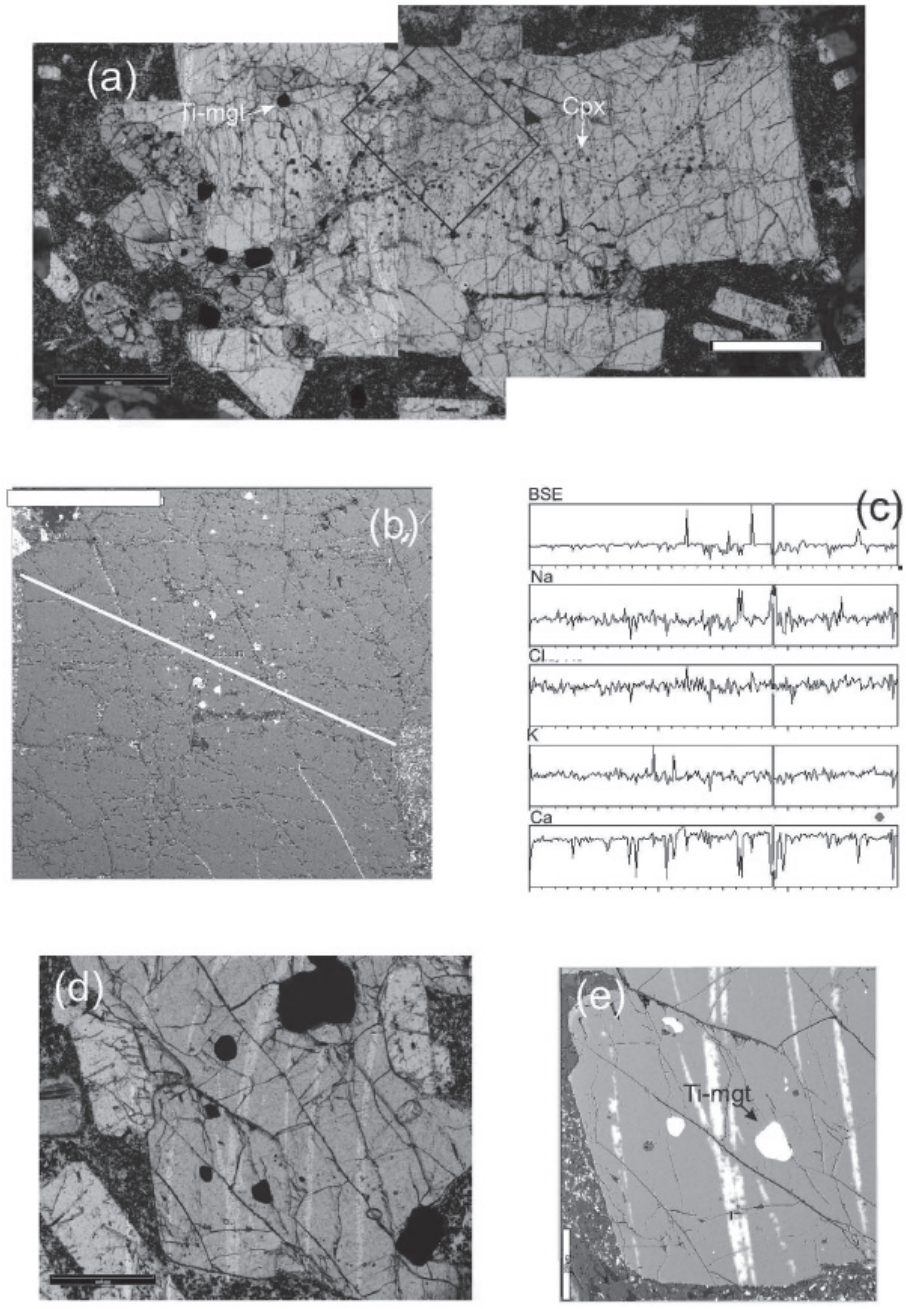


FIG. 5. **a.** Image of plagioclase from sample TC99-5a obtained with a polarised microscope (parallel light) showing small (<10 μ) clinopyroxene (Cpx), Ti-magnetite (Ti-mgt) and fluid and melt inclusions. Scale bar: 0.5 mm; **b.** Scanning electron micrograph (back-scattered electron image) of a selected area of plagioclase phenocryst (see box in a) on which EDX compositional profiles were carried out; **c.** back-scattered topography (BSE) and Na, Cl, K and Ca EDX profiles (total profile length of 2853μ, see b) showing a rather chemical homogeneity; stronger Na and lower Ca variations coincide with small fractures as shown by vertical line in all spectres; **d.** Image of clinopyroxene from sample TC99-5a obtained with a polarised microscope (parallel light); **e.** Scanning electron micrograph (back-scattered electron image) of a selected area of a clinopyroxene phenocryst showing small subidiomorphic Ti-magnetite (Ti-mgt) inclusions; light lamellae are not related to differences in composition but with differences in C sputtering during manipulation of sample.

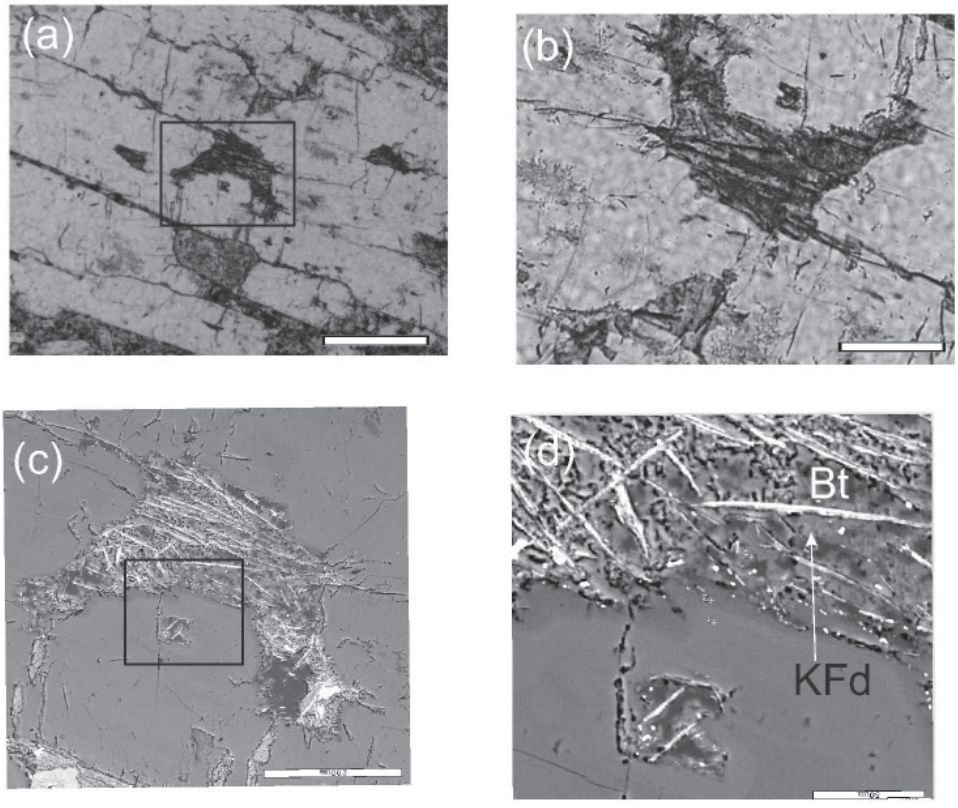


FIG. 6. **a.** Image of plagioclase from sample TC99-2 obtained with a polarised microscope (parallel light) showing small (<25 μ) inclusions. Scale bar: 0.5 mm; **b.** Detail of plagioclase inclusion (scale bar: 0.5 mm); **c.** Scanning electron micrograph (back-scattered electron image) of plagioclase showing inclusions; **d.** Detail of inclusion showing acicular biotites (Bt, EDX analyses) and <20 μ K-feldspar (KFd, light gray). Scale bar: 50 μm.

Plagioclases from sample TC99-2 are also characterised by a rather compositional homogeneity, but small (≈25 μ) inclusions (Figs. 6a, b, c, d) of K-rich domains with acicular biotite and K-feldspar-plagioclase fine intergrown crystals are also present. This type of inclusions is absent in the other studied samples.

Clinopyroxene ($Wo_{37-38}En_{45-39}Fs_{18-23}$, Table 2) from sample TC99-5 presents a rather homogeneous composition, with small inclusions of Ti-magnetite (Figs. 5d, e), classify as augite according to Morimoto *et al.* (1988); its chemistry (*e.g.*, Ti contents) is typical of pyroxene found in calc-alkaline lavas.

## 5. Geochronological Results

### 5.1. $^{40}Ar/^{39}Ar$ results

The bulk sample ARQ99-4 heated by the HF furnace displays a very disturbed age spectrum (Fig. 7a). The apparent ages are clearly correlated with the $^{37}Ar_{Ca}/^{39}Ar_K$ ratio, showing highest ages corresponding to highest $^{37}Ar_{Ca}/^{39}Ar_K$ ratios that represent argon released from the freshest plagioclase. The high temperature $^{37}Ar_{Ca}/^{39}Ar_K$ ratio measured is around 7, in accordance with $^{37}Ar_{Ca}/^{39}Ar_K$ deduced from the Ca/K ratio measured by microprobe (Ca/K=1.83 x $^{37}Ar_{Ca}/^{39}Ar_K$), ranging from 7.0 to 7.9: it corresponds to pure plagioclase. The lowest ages and $^{37}Ar_{Ca}/^{39}Ar_K$ ratios correspond to the degassing of plagioclase and sericite whose presence is already observed in thin sections and SEM images (Fig. 4). The laser experiment on 10 very transparent plagioclase grains displays a plateau age (82% of $^{39}Ar$ released) at 114.1±0.5 Ma corresponding to pure plagioclase fraction, as demonstrated by the constant and higher $^{37}Ar_{Ca}/^{39}Ar_K$ ratios (Table 3). This plateau age matches with the apparent high temperature ages measured with the HF furnace. The inverse isochron

plot $^{39}Ar/^{40}Ar$ *versus* $^{36}Ar/^{40}Ar$ does not give useful information since most of the data are strongly clustered (because of low atmospheric contamination, the first step excepted; age=113.4±1.0 Ma, concordant with the plateau age, atmospheric initial $^{40}Ar/^{36}Ar$ ratio=306.0±17.5, MSWD=2.0). These observations allow considering the plateau age of 114.1±0.5 Ma as geologically reliable and as the best age estimate for the emplacement of this lava flow. Better data obtained with the laser experiment is explained by the low quantity of grains selected that allows a much better choice of pure plagioclase than the bulk sample.

For sample ARQ99-7 (Fig. 7b), one HF furnace and two laser experiments were performed. We observe **1.** a strongly disturbed age spectrum displayed by the HF experiment, and a less disturbed age spectrum on one of the two laser experiments, both with a clear correlation between ages and $^{37}Ar_{Ca}/^{39}Ar_K$ ratios and **2.** a plateau age of 84.3±1.3 Ma for the other laser experiment, corresponding to higher and constant $^{37}Ar_{Ca}/^{39}Ar_K$ ratios. Note that both laser and HF ages and $^{37}Ar_{Ca}/^{39}Ar_K$ ratios converge at high temperature, where pure plagioclase is degassing. This is demonstrated by the $^{37}Ar_{Ca}/^{39}Ar_K$ ratio calculated from the microprobe Ca/K ratios, ranging between 13.4 and 15.5, in good concordance with the highest $^{37}Ar_{Ca}/^{39}Ar_K$ ratios obtained by argon measurements. The inverse isochron plot also characterised by very clustered data (the first step excepted) gives an age of 83.6±1.8 Ma, concordant with the plateau age (initial $^{40}Ar/^{36}Ar$ ratio=316.6±15.8, MSWD=0.7). The plateau age displayed by the laser experiment is probably geologically reliable because of the freshness of the analyzed grains.

The case of sample TC99-2 (Fig. 8a) is similar to that of samples ARQ99-4 and ARQ99-7. **1.** The HF furnace experiment displays a disturbed age spectrum, with a clear correlation between ages and $^{37}Ar_{Ca}/^{39}Ar_K$ ratios, and **2.** the laser experiment shows a plateau age of 91.0±0.6 Ma corresponding to much purer plagioclase. The inverse isochron age, also characterized by clustered points, displays a concordant age of 91.9±0.8 Ma (imprecise initial $^{40}Ar/^{36}Ar$ ratio=236.7±54.1, MSWD=0.5). For the reasons previously given, this plateau age is probably geologically reliable. $^{37}Ar_{Ca}/^{39}Ar_K$ ratios deduced from Ca/K measured with microprobe mainly range between 14.0 and 6.1 (and may occasionally reach 15-20 on cores), that may explain the slightly disturbed $^{37}Ar_{Ca}/^{39}Ar_K$ ratio spectrum corresponding to the plateau age. The disturbed U-like shape of the HF furnace observed could be a consequence of the small acicular biotite and K-feldspar inclusions (Fig. 6) that are always present in these plagioclases.

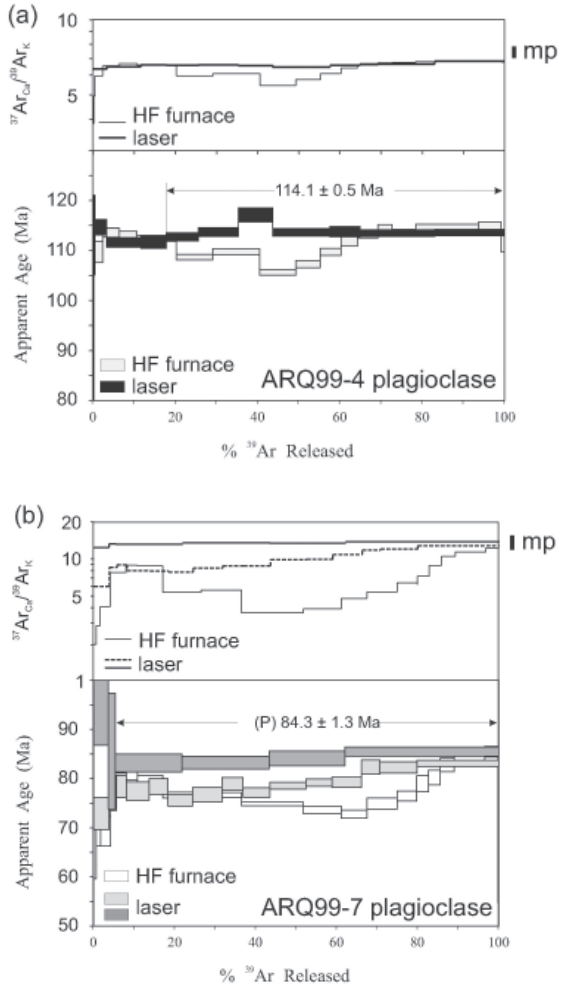


FIG. 7. $^{40}Ar/^{39}Ar$ age and $^{37}Ar_{Ca}/^{39}Ar_K$ ratio spectra obtained on plagioclase bulk samples (HF furnace) and about 10 grains (laser) of plagioclase from **(a)** a lava flow (sample ARQ99-4) and **(b)** a dyke (ARQ99-7) from the Lower Cretaceous volcanism of the Coastal Range in La Serena area (sector A in Fig. 1). In sample ARQ99-7, two different laser measurements (shown with different grey tone in the spectra) were carried out. In all cases, plateau (P) ages are given at the 2σ level whereas the error bar on apparent ages are given at the 1σ level. mp= $^{37}Ar_{Ca}/^{39}Ar_K$ calculated from Ca/K ratios from microprobe analyses (Table 1).

Finally, for sample TC99-5A (Fig. 8b), both HF furnace and laser heating experiments display disturbed age spectra, although the $^{37}Ar_{Ca}/^{39}Ar_K$ ratios are constant in both cases (low temperature steps excepted) and consistent with the $^{37}Ar_{Ca}/^{39}Ar_K$ ratio calculated from Ca/K measured with microprobe (from 7.7 for albitic rims, to 12.4 for the more calcic cores). The only (but important for the interpretation) difference between the two results is that the laser experiment displays a U shaped age spectrum, whereas the HF furnace data show more or less regularly increasing apparent ages at low and intermediate temperature. At higher temperature, furnace heating data show nearly constant apparent ages around 117.0±0.6 Ma (weighted mean calculated on seven steps, ≈50% Ar released). The laser heating experiment presents even more stable apparent ages at high temperature, with a weighted mean age of 115.3±0.5 Ma (7 steps, 56% of $^{39}Ar$ released, not concordant with furnace heating data). At lowest temperatures, ages are nicely correlated with $^{37}Ar_{Ca}/^{39}Ar_K$ ratios for the furnace experiment, demonstrating the degassing of secondary K-rich alteration minerals. In contrast, laser heating experiments show dominant higher ages at low temperature, corresponding to much less disturbed $^{37}Ar_{Ca}/^{39}Ar_K$ ratios. Therefore, the laser experiment age spectrum represents nearly pure plagioclase, whereas the furnace heating data are more affected by alteration processes on plagioclase. This allows interpreting the laser heating experiment, showing a slight (but clear) saddle shaped age spectrum, as representing the plagioclase itself that appears affected by slight excess $^{40}Ar$. This U-shape, characteristic of excess argon, is not visible at low temperature for the furnace heating data, because of the existence of secondary K-rich minerals that decrease the apparent ages. Such plagioclase age spectrum, with the U shape mostly concentrated in the first half of the spectrum, is not very frequent but has been previously reported in the case of plagioclase unambiguously affected by excess argon (Le Gall *et al.*, 2002; Lenoir *et al.*, 2003). In this case, the weighted mean age calculated from the three minimum apparent ages for the laser heating experiment (111.3±0.9 Ma, Fig. 8b), represents a maximum age for the emplacement of this rock. This age is concordant with the weighted mean calculated on two intermediate temperature steps of the furnace data (112.3±0.6 Ma). Note that on the opposite, the corresponding high temperature ages are not concordant. Because of the apparent low disturbance induced by this excess $^{40}Ar$, it is likely that these weighted mean ages are not far from the true age of this sample.

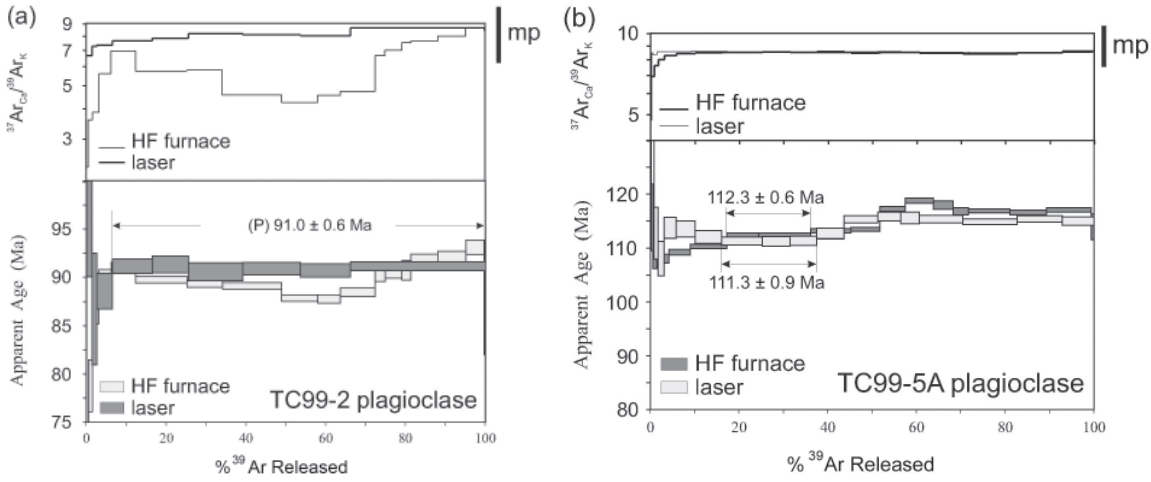


FIG. 8. $^{40}Ar/^{39}Ar$ age and $^{37}Ar_{Ca}/^{39}Ar_K$ ratio spectra obtained on plagioclase bulk samples (HF furnace) and 13-80 grains (laser) of plagioclase from two lava flows: **a.** sample TC99-2 and **b.** sample TC99-5a from the Lower Cretaceous volcanism of the Coastal Range in La Serena area (sector B in Fig. 1). In all cases, ages are given at the 2σ level whereas the error bar for apparent ages are given at the 1σ level. mp: $^{37}Ar_{Ca}/^{39}Ar_K$ calculated from Ca/K ratios from microprobe analyses (Table 1).

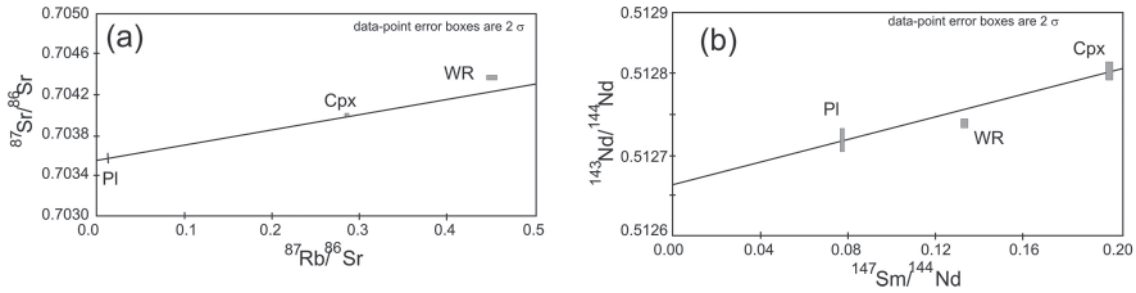


FIG. 9. **a.** Rb/Sr isochron diagram obtained from sample TC99-5a (**WR:** whole-rock; **Pl:** plagioclase; **Cpx:** clinopyroxene); **b.** Sm/Nd isochron diagram obtained from sample TC99-5a (**WR:** whole-rock; **Pl:** plagioclase; **Cpx:** clinopyroxene).

### 5.2. Rb/Sr and Sm/Nd isotopic results

Rb/Sr and Sm/Nd isotopic ratios of clinopyroxene, plagioclase and whole-rock from sample TC99-5a are given in table 4 and plotted in a $^{87}Rb/^{86}Sr$ *versus* $^{87}Sr/^{86}Sr$ (Fig. 9a) and a $^{147}Sm/^{144}Nd$ *versus* $^{143}Nd/^{144}Nd$ (Fig. 9b) diagram. An apparent age of 106.0±5.3 Ma (2σ) with $(^{87}Sr/^{86}Sr)_o$=0.70356±0.00002 is obtained with the Rb-Sr methodology using plagioclase and clinopyroxene data only, whereas an age of 116±16 Ma (2σ) with $(^{143}Nd/^{144}Nd)_o$=0.512667±0.000018 is obtained from the Sm-Nd data on the same minerals. In both isotopic systems, whole-rock data plot outside the internal isochron, probably due to the low-temperature alteration processes affecting the sample or to some kind of isotopic heterogeneity between phenocrysts and whole-rock. When whole-rock data are also plotted, errorchrons (without geological meaning) are obtained (124±180 Ma in the Rb/Sr isochron and 119±360 Ma in the Sm/Nd isochron). As recently demonstrated by Davidson *et al.* (2005), independent age estimates are needed to evaluate isotopic data if determination of isochron ages in volcanic rocks would be made. However, initial isotopic values obtained from the isochron (≈0.70356) would be useful for petrogenetic constraints.

## 6. Discussion and Conclusions

### 6.1. The geochronological data

As shown in figures 7a, 7b and 8a, partial alteration (mostly sericitization) of plagioclase clearly disturbed the age spectra of samples ARQ99-4 ARQ99-7 and TC99-2. However, laser heating determinations involving a much smaller quantity of grains carefully selected, could display plateau ages corresponding to pure plagioclase, as demonstrated by a constant $^{37}Ar_{Ca}/^{39}Ar_K$ ratio. These plateau ages correspond to high temperature ages obtained with furnace heating. Moreover, the good concordance between the $^{37}Ar_{Ca}/^{39}Ar_K$ measured and the Ca/K ratio obtained by microprobe analysis indicates that both the laser heating plateau ages and the high temperature apparent ages obtained on bulk sample and small grain clusters probably represent the best crystallization age determination for these rocks. Sample TC99-5a, corresponding to mostly fresh plagioclase (laser and furnace heating) is probably affected by low amount of excess $^{40}Ar$. Its best age estimate is given by the lowest intermediate temperature ages of the laser heating experiment. For TC99-5a Rb/Sr and/or Sm/Nd internal isochrones (Fig. 9a and b), high error bars are obtained when using clinopyroxene, plagioclase and whole-rock, as a consequence of **1.** the low concentrations of Rb, Sm and Nd in plagioclase and clinopyroxene, **2.** the different mobility of Rb (and also Sr) in whole-rock and plagioclase due to alteration and/or **3.** the absence of initial isotopic equilibrium between minerals and groundmass. However, when plotting phenocrysts only, calculated isochron ages match with the best $^{40}Ar/^{39}Ar$ radiometric estimations. This is in accordance with the absence of initial isotopic equilibrium between minerals in volcanic rocks, as demonstrated by Davidson *et al*. (2005). These authors have shown differences in the initial isotopic ratio at the mineral scale which can result in erroneous or imprecise ages when using the isochron method. In these cases, independent knowledge of ages using precise geochronological methods (*e.g.*, $^{40}Ar/^{39}Ar$) is needed.

These new radiometric $^{40}Ar/^{39}Ar$ ages are inconsistent with the Hauterivian-Upper Barremian age (around 125-136 Ma, Geologic time scale of the International Commission on Stratigraphy, 2004) assigned to the calcareous units of the studied area based on palaeontological and biostratigraphic data (Pérez and Reyes, 2000; Mourgues, 2000a, b, c). This discrepancy is hardly explained by too young Ar/Ar ages because although the rocks are affected by alteration, the obtained results do not show any evidence of partial resetting of the K-Ar system on the freshest plagioclase phases. Nevertheless, according to the limited radiometric data available it would be useful to get more detailed geochronological work to more accurately determine the age of both volcanic and sedimentary rocks.

### 6.2. Duration of the volcanism

The Lower Cretaceous is characterized by the presence of huge volumes of subaerial lavas intercalated with shallow marine sediments. These lavas have a high geochemical homogeneity, with high $Al_2O_3$ and low MgO values, classifying as high-K to shoshonitic basaltic andesites and andesites. Their trace element patterns are typical of magmas erupted in an extensional and progressively attenuated intra arc basin (Levi *et al*., 1988; Vergara *et al*., 1995; Morata *et al*., 2001).

Previous precise $^{40}Ar/^{39}Ar$ analyses of plagioclase from this Lower Cretaceous Volcanic Province displayed plateau ages of 119.4±2.4 (2σ) and 118.7±0.6 Ma (2) in lavas belonging to the Veta Negra Formation, at the 33°25' and 33°S, respectively (Aguirre *et al*, 1999; Fuentes *et al.*, 2005), leading these authors to propose that most of this huge volcanic province in this part of the Coastal Cordillera was mostly emplaced around 119 Ma. The present geochronological data concerning the northern region of La Serena, if valid, show younger ages, apparently indicating a much longer duration of the volcanism. Ages of 114.1±0.5 Ma (sample ARQ99-4), and 111.3±0.9 Ma (sample TC99-5a), 91.0±0.6 Ma (sample TC99-2) were found on lava flows, and 84.3±1.3 Ma on a dyke (sample ARQ99-7). All these dated volcanic rocks and those from the southern areas previously studied have relatively homogeneous geochemical signatures (Morata and Aguirre, 2003), except for sample TC99-2, that is isotopically more primitive (Fig. 10). A longer duration of the volcanism in La Serena region as compared with the southern areas according with the available published ages, is in agreement with the existence of abundant interlayered shallow marine sediments, whereas continuous and thick lava flows, with minor intercalations of continental sediments, characterize the southern regions that seem to have been generated by a huge and a brief magmatic event. All these features would be comparable to those characterizing other igneous provinces like those from the Jurassic-Early Cretaceous in northern Chile (Lucassen *et al*., 2006; Oliveros *et al*., 2006).

### 6.3. Geodynamic implications

The rocks of both La Serena region and the southern areas (Veta Negra Formation at the Bustamante and Chacana areas) are characterized by high-K calcalkaline basalts to basaltic andesites, with a marked Nb-Ta trough typical of arc magmas and with similar initial isotopic ratios. Morata *et al.* (2001, 2003) and Morata and Aguirre (2003) have explained these characteristics as the result of a relatively high and constant degree of partial melting from a rather homogeneous basaltic source. Based on their geochemical signature, an extensional geodynamic setting has been previously proposed by Aguirre *et al.* (1989), Vergara *et al.* (1995), Morata and Aguirre (2003) as the dominant regime during genesis of this volcanism.

A low-spreading rate of 5 $cmyr^{-1}$ in the SE Pacific during the interval 125-110 Ma as proposed by Larson and Pitman (1972), would increase the subduction angle at the South American Pacific margin. On this scenario, partial melting under low-pressure conditions, due to the attenuated thickness of the continental crust during this period as a consequence of the dominant extensional regime, would be favoured (Morata and Aguirre, 2003).

Sample TC99-2, dated at 91.0±0.6 Ma and having a more primitive isotopic signature (Fig. 10) could represent the end of the Early Cretaceous extensional event in this region. On the other hand, the youngest dyke sample ARQ99-7 (84.3±1.3 Ma), with geochemical features similar to those of the *ca.* 119 Ma old lava flows from central Chile (Fig. 10), could indicate a later distinct magmatic pulse. This last magmatic pulse could belong to the Upper Cretaceous Viñita Formation volcanism, which erupted at the beginning

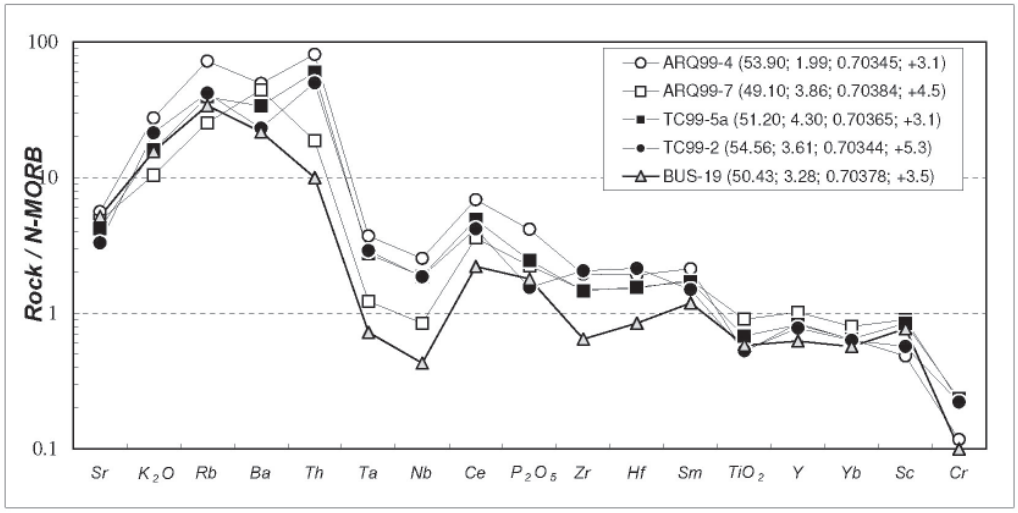


FIG. 10. Rock/N-MORB (Pearce, 1982) normalised diagram for trace elements of dated samples (ICP-MS data, Morata and Aguirre, 2003) of the Coastal Range of La Serena Region. Sample BUS-19 belong to the Veta Negra Formation at the Bustamante Hill (data from Vergara *et al.,* 1995) dated by Aguirre *et al.* (1999) by $^{40}Ar/^{39}Ar$ in plagioclase at 119.4±2.4 (2σ) Ma. In parentheses, values of $\%SiO_2$, %MgO; $(^{87}Sr/^{86}Sr)_o$ and εNd.

of the Late Cretaceous, and is characterized by a similar geochemistry (Morata *et al.,* 2003).

In conclusion, these new $^{40}Ar/^{39}Ar$ ages allow a better constraint of the extensional magmatism during the Early Cretaceous in the Coastal Range of central and north-central Chile. Differences are observed between the timing of volcanism in central Chile, mostly around 119 Ma, and the more episodic volcanism at La Serena latitude. Moreover, in La Serena region volcanism is partially coeval with plutonism (as deduced from published K-Ar ages, Emparan and Pineda, 2000, Fig. 1), whereas at the latitude of Santiago, the bulk of the volcanism clearly predates plutonism (Aguirre *et al*., 2002; Parada *et al.*, 2005). All these data could be in agreement with a long lived Early Cretaceous Igneous Province (119-84 Ma), that could have started with a huge magmatic event in present day central Chile, followed by smaller and discrete magmatic pulses further north.

## Acknowledgements

This study was supported by the Departamento de Investigación y Desarrollo (DID), Universidad de Chile, Project I001-99/2, FONDECYT Projects 1031000, 7040160 and 7050282, the Spanish project BTE-2003-06265 (Ministry of Science and Technology/Ministry of Education and Science and FEDER), the RNM 131 of Junta de Andalucía and the 'Plan Propio' of Granada University. The authors thank F. Bea and P. Montero (Granada University) for the facilities in the isotopic and ICP-MS analyses and to J. Vargas (Universidad de Chile) for their hard work in the separation of plagioclase and clinopyroxene phenocrystals. We also thank C. Mpodozis (Antofagasta Minerals), S. Nomade (Laboratoire des Sciences du Climat et de l' Environnement) and an anonymous referee for their helpful comments on an early version of this manuscript.

## References

Aguirre, L. 1985. The Southern Andes. *In* The ocean basins and margins: The Pacific Ocean (Nairn, A.E.M.; Stehli, F.G.; Uyeda, S.; editors). Plenum Press 7a: 265-376. New York.

Aguirre, L.; Egert, E. 1965. Cuadrángulo Quebrada Marquesa, provincia de Coquimbo. Instituto de Investigaciones Geológicas, Carta Geológica de Chile 15: 92 p., 1 mapa 1:50.000.

Aguirre, L.; Egert, E. 1970. Cuadrángulo Lambert (La Serena), provincia de Coquimbo. Instituto de Investigaciones Geológicas, Carta Geológica de Chile 23: 14 p.

Aguirre, L.; Féraud, G.; Morata, D.; Vergara, M.; Robinson, D. 1999. Time interval between volcanism and burial metamorphism and rate of basin subsidence in a Cretaceous Andean extensional setting. Tectonophysicis 313: 433-447.

Aguirre, L.; Levi, B.; Nyström, J.O. 1989. The link between metamorphism, volcanism and geotectonic setting during the evolution of the Andes. Geological Society of London, Special Publications 43: 223-232.

Aguirre, L.; Parada, M.A.; Morata, D.; Féraud, G.; Fuentes, F. 2002. Compositional features and geodynamic evolution of volcanic and plutonic components in the Lower Cretaceous magmatic province (coastal range of Central Chile). *In* International Symposium on Andean Geodynamics (ISAG), No. 5, 2002: 19-22. Toulouse.

Boric, R.; Munizaga, F. 1994. Geocronología Ar-Ar y Rb-Sr del depósito estratoligado de cobre El Soldado (Chile central). Comunicaciones 45: 135-148.

Davidson, J.; Charlier, B.; Hora, J.M.; Perlroth, R. 2005. Mineral isochrons and isotopic fingerprinting: Pitfalls and promises. Geology 33 (1): 29-32.

Drake, R.; Vergara, M.; Munizaga, F.; Vicente, J.C. 1982. Geochronology of Mesozoic-Cenozoic magmatism in central Chile, Lat. 31°-36°S. Earth-Science Reviews 18: 353-363.

Emparan, C.; Pineda, G. 1999. Área Condoriaco-Rivadavia, Región de Coquimbo. Servicio Nacional de Geología y Minería, Mapas Geológicos 12, escala 1:100.000.

Emparan, C.; Pineda, G. 2000. Área La Serena-La Higuera, Región de Coquimbo. Servicio Nacional de Geología y Minería, Mapas Geológicos 18, escala 1:100.000.

Emparan, C.; Pineda, G. 2006. Geología del Área Andacollo-Puerto Aldea, Región de Coquimbo. Servicio Nacional de Geología y Minería, Carta Geológica de Chile, Serie Geología Básica 96: 85 p. 1 mapa escala 1:100.000.

Fuentes, F.; Féraud, G.; Aguirre, L.; Morata, D. 2001. Convergent strategy to date metamorphic minerals in subgreenschit facies metabasites by the $^{40}Ar/^{39}Ar$ method. *In* South American Symposium on Isotope Geology No. 3, Extended Abstracts Volume (CD), Sociedad Geológica de Chile: 34-36.

Fuentes, F.; Féraud, G.; Aguirre, L.; Morata, D. 2005. $^{40}Ar/^{39}Ar$ dating of volcanism and subsequent very low-grade metamorphism in a subsiding basin: example of the Cretaceous lava series from central Chile. Chemical Geology 214: 157-177.

Jourdan, F.; Verati, C.; Féraud, G. 2006. Intercalibration of the Hb3gr $^{40}Ar/^{39}Ar$ dating standard. Chemical Geology 231: 177-189.

Larson, R.L.; Pitman, W.C. 1972. World wide correlation of Mesozoic magnetic anomalies, and its implications. Geological Society of America Bulletin 83: 3645-3662.

Le Gall, B.; Tshoso, G.; Jourdan, F.; Féraud, G.; Bertrand, H.; Tiercelin, J.J.; Kampunzu, H.; Modisi, M.P.; Dyment, J.; Maia, M. 2002. $^{40}Ar/^{39}Ar$ geochronology and structural data from the giant Okavango and related mafic dyke swarms, Karoo igneous province, Botswana. Earth and Planetary Science Letters 202: 595-606.

Lenoir, X.; Féraud, G.; Geoffroy, L. 2003. High-rate flexuring of the East Greenland volcanic margin: constraints from $^{40}Ar/^{39}Ar$ datings of basaltic dykes. Earth and Planetary Science Letters 214: 515-528.

Levi, B.; Nyström, J.O.; Thiele, R.; Åberg, G. 1988. Geochemical trends in Mesozoic-Tertiary volcanic rocks from the Andes in Central Chile and tectonic implications. Journal of South American Earth Sciences 1 (1): 63-74.

Levi, B.; Aguirre, L.; Nyström, J.O.; Padilla, H.; Vergara, M. 1989. Low-grade regional metamorphism in the Mesozoic-Cenozoic volcanic sequences of the Central Andes. Journal of Metamorphic Geology 7: 487-495.

Lucassen, F.; Kramer, W.; Bartsch, V.; Wilke, H.G.; Franz, G.; Romer, R.L.; Dulski, P. 2006. Nd, Pb and Sr isotope composition of juvenile magmatism in the Mesozoic large magmatic province of northern Chile (18-27°S): indications for a uniform subarc mantle. Contributions to Mineralogy and Petrology 152: 571-589.

Ludwig, K.R. 2000. Using Isoplot/Ex. A geochronological toolkit for Microsoft Excel. Berkeley Geochronology Center, Special Publication 1. Berkeley.

Morata, D.; Aguirre, L. 2003. Extensional Lower Cretaceous volcanism in the Coastal Range (29°20'-30°S), Chile: geochemistry and petrogenesis. Journal of South American Earth Sciences 16: 459-476.

Morata, D.; Aguirre, L.; Féraud, G.; Fuentes, F.; Parada, M.A.; Vergara, M. 2001. The Lower Cretaceous volcanism in the Coastal Range of central Chile: geochronology and isotopic geochemistry. *In* South American Symposium on Isotope Geology No. 3, Extended Abstracts Volume (CD), Sociedad Geológica de Chile: 321-324.

Morata, D.; Aguirre, L.; Belmar, M.; Morales, S.; Parada, M.A.; Martínez, M.; Carrillo, J. 2003. Geochemical evolution of the Cretaceous magmatism in the Coastal Range of the La Serena (30°S). *In* Congreso Geológico Chileno No. 10, Actas (CD). Concepción.

Morimoto, N.; Fabries, J.; Ferguson, A.K.; Ginzburg, I.V.; Ross, M.; Seifert, F.A.; Zussman, J.; Aoki, K.; Gotardi, G. 1988. Nomenclature of pyroxenes. American Mineralogist 73 (9-10): 1123-1133.

Moscoso, R. 1976. Antecedentes sobre un engranaje volcánico-sedimentario marino del Neocomiano en el área de Tres Cruces, IV región, Chile. *In* Congreso Geológico Chileno, No. 1, Actas 1: 155-167

Mourgues, A. 2000a. Bioestratigrafía de las facies calcáreas marinas de las formaciones Arqueros y Quebrada Marquesa, IV Región, Chile. *In* Congreso Geológico Chileno No. 9, Actas 1: 519-523. Puerto Varas.

Mourgues, A. 2000b. Correlación de la sucesión clástica calcárea de la Quebrada de Los Choros con la Formación Arqueros, sobre la base de su contenido faunístico, litología y relaciones de contacto, IV Región, Chile. *In* Congreso Geológico Chileno No. 9, Actas 1: 524-527. Puerto Varas.

Mourgues, A. 2000c. Fauna de ammonites crioceratidos del Hauteriviano superior provenientes de Agua de Pajaritos, Quebrada de Los Choros, norte de La Serena, IV Región, Chile. *In* Congreso Geológico Chileno No. 9, Actas 1: 528-531. Puerto Varas.

Mourgues, F.A. 2004. Advances in ammonite biostratigra-

phy of the marine Atacama basin (Lower Cretaceous), northern Chile, and its relationship with the Neuquén basin, Argentina. Journal of South American Earth Sciences 17: 3-10.

Munizaga, F.; Holmgren, C.; Huete, C.; Kawashita, K. 1988. Geocronología de los yacimientos de cobre El Soldado y Lo Aguirre, Chile central. *In* Congreso Geológico Chileno No. 5, Actas 3: 177-193. Santiago.

Oliveros, V.; Féraud, G.; Aguirre, L.; Morata, D. 2006. The Early Andean Magmatic Province (EAMP): $^{40}Ar/^{39}Ar$ dating on Mesozoic volcanic and plutonic rocks from the Coastal Cordillera, Northern Chile. Journal of Volcanological and Geothermal Research 157: 311-330.

Palmer, H.C.; Hayatsu, A.; MacDonald, W.D. 1980. Palaeomagnetic and K-Ar age studies of a 6 km-thick Cretaceous section from the Chilean Andean. Geophysical Journal of the Royal Astronomical Society 63: 133-153.

Parada, M.A.; Féraud, G.; Fuentes, F.; Aguirre, L.; Morata, D.; Larrondo, P. 2005. Ages and cooling history of the Early Cretaceous Caleu pluton: testimony of a switch from a rifted to a compressional continental margin in central Chile. Journal of the Geological Society 162: 273-287.

Pearce, J.A. 1982. Trace elements characteristics of lavas from destructive plate boundaries. *In* Andesites. Orogenic andesites and related rocks (Thorpe, R.S.; editor). John Willey and Sons: 525-548.

Pérez, E.; Reyes, R. 2000. Nuevos antecedentes paleontológicos sobre la edad de los miembros sedimentarios marinos de las formaciones Arqueros y Quebrada Marquesa, norte y sur del río Elqui, IV Región, Chile. *In* Congreso Geológico Chileno No. 9, Actas 1: 532-536. Puerto Varas.

Pineda, G.; Emparan, C. 1997. Nuevos antecedentes de la estratigrafía y geocronología del norte del río Elqui: Evidencias de tectónica extensional. *In* Congreso Geológico Chileno No. 8, Actas 1: 215-219. Antofagasta.

Renne P.R.; Swisher, C.C.; Deino, A.L.; Karner, D.B.; Owens, T.; de Paolo, D.J. 1998. Intercalibration of Standards, absolute ages and uncertainties in $^{40}Ar/^{39}Ar$ dating. Chemical Geology Isotope Geoscience Section 145: 117-152.

Rivano, S.; Sepúlveda, P.; Boris, R.; Espiñeira, D. 1993. Hojas Quillota y Portillo, Región de Valparaíso. Servicio Nacional de Geología y Minería, Carta Geológica de Chile No. 73, 1 mapa escala 1:250.000. Texto inédito 'Geología de las Hojas Quillota y Portillo' (Rivano, 1996).

SERNAGEOMIN. 1982. Mapa Geológico de Chile. Servicio Nacional de Geología y Minería, 1 mapa Geológico en 3 hojas, escala 1:1.000.000.

Tegner, C. 1997. Iron in plagioclase as a monitor of the differentiation of the Skaergaard intrusion. Contributions to Mineralogy and Petrology 128: 45-51.

Turner, G.; Huneke, J.C.; Podose, F.A.; Wasserburg, G.J. 1971. $^{40}Ar/^{39}Ar$ ages and cosmic ray exposure ages of Apollo 14 samples. Earth and Planetary Science Letters 12: 19-35.

Vergara, M.; Levi, B.; Nyström, J.; Cancino, A. 1995. Jurassic and Early Cretaceous island arc volcanism, extension, and subsidence in the Coast Range of central Chile. The Geological Society of America Bulletin 107: 1427-1440.

Vergara, M.; Nyström, J. 1996. Geochemical features of Lower Cretaceous back-arc lavas in the Andean Cordillera, Central Chile (31-34°S). Revista Geológica de Chile 23 (1): 97-106.

Manuscript received: October 20, 2006; accepted: June 6, 2007.